

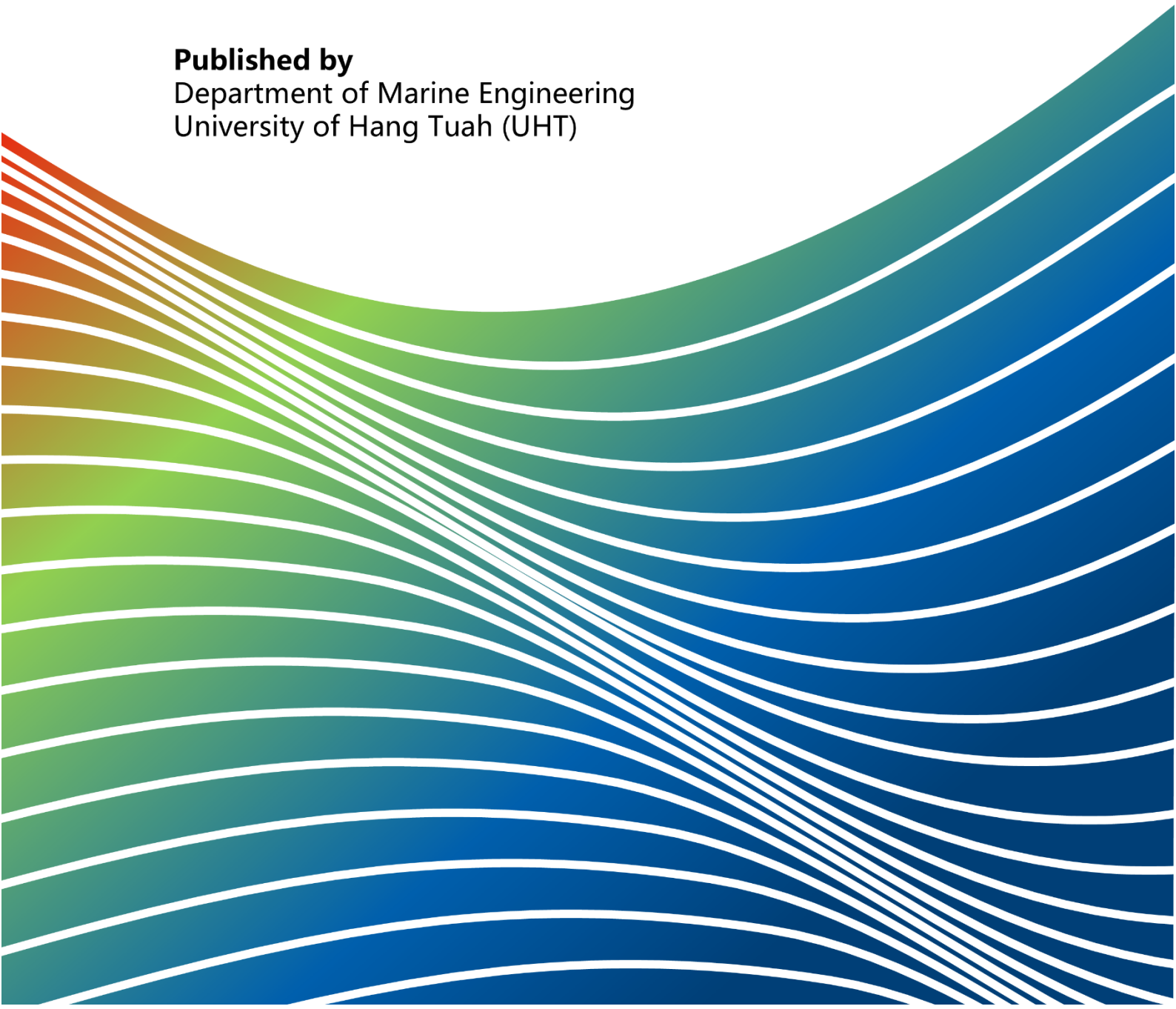
Volume 2
Number 2

September 2025

eISSN: 3063-640X

INTERNATIONAL JOURNAL OF **MARINE ENGINEERING AND APPLICATIONS**

Published by
Department of Marine Engineering
University of Hang Tuah (UHT)



INTERNATIONAL JOURNAL OF MARINE ENGINEERING AND APPLICATIONS

VOLUME 2, NUMBER 2, SEPTEMBER 2025

DOI:

TABLE OF CONTENTS

ARTICLE

- | | |
|--|---------------|
| ANALYSIS OF THE EFFECT OF THE SECOND THICKNESS LAYER OR INTERMEDIATE LAYER ON THE THREE-LAYER SYSTEM ON ADHESION STRENGTH ON CARBON STEEL SURFACE | 60-70 |
| Soni Rusmana, Tri Agung Kristiyono, Ali Azhar, Intan Baroroh, Didik Hardianto | |
| DOI: https://doi.org/10.30649/ijmea.v2i2.384 | |
| PERFORMANCE EVALUATION OF SCR (SELECTIVE CATALYTIC REDUCTION) SYSTEM REDUCING EMISSIONS IN SHIP MAIN ENGINES | 71-77 |
| Muhammad Naim, Sugeng Marsudi | |
| DOI: https://doi.org/10.30649/ijmea.v2i2.385 | |
| PREHEATING TEMPERATURE EFFECT ON FLUX-CORED ARC WELDING (FCAW) IN 3G POSITION ON STEEL PLATE TOWARDS TENSILE STRENGTH AND HARDNESS | 78-88 |
| Shihab Maulana Imam Saputra, Dwisetiono, Urip Prayogi, Arif Winarno, Maxima Ari Saktiono | |
| DOI: https://doi.org/10.30649/ijmea.v2i2.388 | |
| THE EFFORTS TO IMPROVE REPAIR AND MAINTENANCE ON THE SHIP ENGINE TO OVERCOME OVER NOISE | 89-93 |
| Cahya Kusuma, Mahendra Indriaryanto | |
| DOI: https://doi.org/10.30649/ijmea.v2i2.389 | |
| MATERIAL DURABILITY ANALYSIS ON FIBERGLASS SHIP CONSTRUCTION | 94-101 |

Fariz Maulana Noor

DOI: <https://doi.org/10.30649/ijmea.v2i2.394>

**DESIGN OF THE MAIN ENGINE FOUNDATION OF SHIP X TO SUPPORT
MAIN ENGINE REPOWERING**

102-110

Agil Thoriq Ramadhani, Sutrisno

DOI: <https://doi.org/10.30649/ijmea.v2i2.396>

**SUSTAINABLE MARITIME HUMAN RESOURCE DEVELOPMENT
STRATEGY IN SUPPORTING THE BLUE ECONOMY IN INDONESIA**

111-117

Dedi Kristiawan, Sugeng Marsudi

DOI: <https://doi.org/10.30649/ijmea.v2i2.393>

INTERNATIONAL JOURNAL OF MARINE ENGINEERING AND APPLICATIONS

EDITORIAL BOARDS

EDITOR IN CHIEF

Dr. Arif Winarno, S.T., M.T.

Department of Marine Engineering, Universitas Hang Tuah, Indonesia

ASSOCIATE EDITORS

Dr. Ir. Frengki Mohamad Felayati, S.T.

Department of Marine Engineering, Universitas Hang Tuah, Indonesia

EDITOR MEMBER

Dr. Sutrisno, S.T., M.T.

Department of Marine Engineering, Universitas Hang Tuah, Indonesia

Erik Sugianto, S.T., M.T., Ph.D.

Department of Marine Engineering, Universitas Hang Tuah, Indonesia

Dr. Eng. Deddy Chrismianto, S.T, M.T.

Department of Naval Architecture, Universitas Diponegoro, Indonesia

Dr. Eng. Mohammad Danil Arifin, S.T., M.T.

Department of Marine Engineering, Universitas Darma Persada, Indonesia

Date of Received:
June 28, 2025

Date of Accepted:
September 1, 2025

Date of Published:
September 30, 2025
DOI: doi.org/10.30649/ijmea.v2i2.384

ANALYSIS OF THE EFFECT OF THE SECOND THICKNESS LAYER OR INTERMEDIATE LAYER ON THE THREE-LAYER SYSTEM ON ADHESION STRENGTH ON CARBON STEEL SURFACE

Soni Rusmana^{1*}, Tri Agung Kristiyono¹, Ali Azhar¹, Intan Baroroh¹, Didik Hardianto¹

¹ Department of Naval Architecture and Shipbuilding, Hang Tuah University, 60111, Indonesia

*Corresponding Author: rusmanasoni88@gmail.com

ABSTRACT

Generally, the marine & offshore industry uses a wide range of coatings, both liquid and thermal, which aim to protect or inhibit the rate of corrosion of materials in the surrounding environment. Referring to the Norsok M-501 standard, there is a Coating System Data Sheet (CSDS) that provides an overview of the coating system according to the surrounding environment. In CSDS 1B, a three-layer system is employed, consisting of a zinc-rich epoxy primary layer, an epoxy intermediate layer, and a UV-resistant top layer. The specification provides the thickness of each coating layer from the first layer to the top layer. However, during the fabrication process, there are some challenges that occur with the second layer, which is epoxy. Sometimes, during the application of the second layer, the thickness of this layer is less than or more than the specified thickness. This study aims to determine the effect of the thickness of the second layer (intermediate layer), namely epoxy, on the adhesion of the three-layer system. This research will be carried out through experimental testing with variations in the thickness of the second layer (intermediate coat) of 50, 100, 150, 200, and 250 microns. The adhesion test for the second layer will use the X-Cut Tape Test and Pull-Off Test methods. The results of the adhesion strength test show that the thickness of the second layer affects the adhesion value of the coating system itself; The thicker the intermediate layer, the worse the adhesion strength, or there is a decrease in adhesion strength. This is supported by the test results on panel 1 with a second layer thickness of 50 microns, which obtained an average tensile test result of 18.37 MPa, and on panel 5 with a second layer thickness of 250 microns, which obtained an average tensile test result of 14.19 MPa.

Keywords: Coating, intermediate layer, pull-off test, three-layer system, x-cut tape test

Introduction

In the marine and offshore industries, steel is a major material widely used for structural construction because it has high strength and abundant availability. However, steel is particularly susceptible to corrosion due to exposure to the aggressive marine environment. Corrosion is one of the main causes of structural damage, increased maintenance costs, and disruption to safety and operational continuity. Therefore, mitigation efforts through surface coating systems have become a key strategy that

continues to be developed to protect metal structures, particularly in marine installations [1]. As the need for reliable maritime infrastructure increases, both globally and nationally, industry attention is now focused on the effectiveness of corrosion protection systems that are able to adapt to extreme conditions. Oil and gas exploration and production in the deep sea, as well as the development of ports and marine facilities in tropical regions such as Indonesia, make the study of coating systems increasingly relevant. In the national context, this urgency is reinforced by the increasing economic value of Indonesia's marine

and fisheries sectors, which directly require durable structures and minimal maintenance [2].

Various international standards, such as NORSOK M-501, have recommended specific coating systems, one of which is the CSDS 1B system, which consists of three layers of protection. However, there is still a gap in understanding the actual performance of these coating systems, especially regarding the thickness of each layer, the order of application, and their adaptability to tropical environmental conditions that have high humidity and significant chloride levels. Previous studies have examined the effectiveness of coating with zinc-rich epoxy bases, pure epoxy, and UV-resistant top coatings, but the results still show inconsistencies, especially in terms of thickness optimization and the influence of environmental conditions on corrosion resistance [3, 4].

In addition, most of the previous studies were conducted in temperate or polar environments, so their relevance to Indonesia's tropical climatic conditions has not been thoroughly verified. The lack of comprehensive studies linking technical data in the field to the effectiveness of coating systems recommended by international standards suggests that evaluation of CSDS 1B systems in local contexts is still urgently needed. Taking into account the differences in environmental characteristics, it is important to know the extent to which existing coating systems can guarantee optimal protection of steel structures [5, 6].

Based on this background, this study aims to evaluate and analyze the performance of the CSDS 1B coating system on steel structures in tropical marine environmental conditions. This research will focus on the thickness of the coating, the order of its application, and its effectiveness in preventing corrosion according to the conditions found in Indonesia's maritime area. The results of this study are expected to contribute to the development of a more contextually appropriate and effective corrosion protection system.

Methodology

a. Flow Chart

This study aims to investigate the adhesion strength of coatings on carbon steel surfaces with varying intermediate paint thicknesses. The methodology is systematically illustrated in a flowchart (Figure 1) and starts with basic steps before moving through the preparation, testing, and analysis phases.

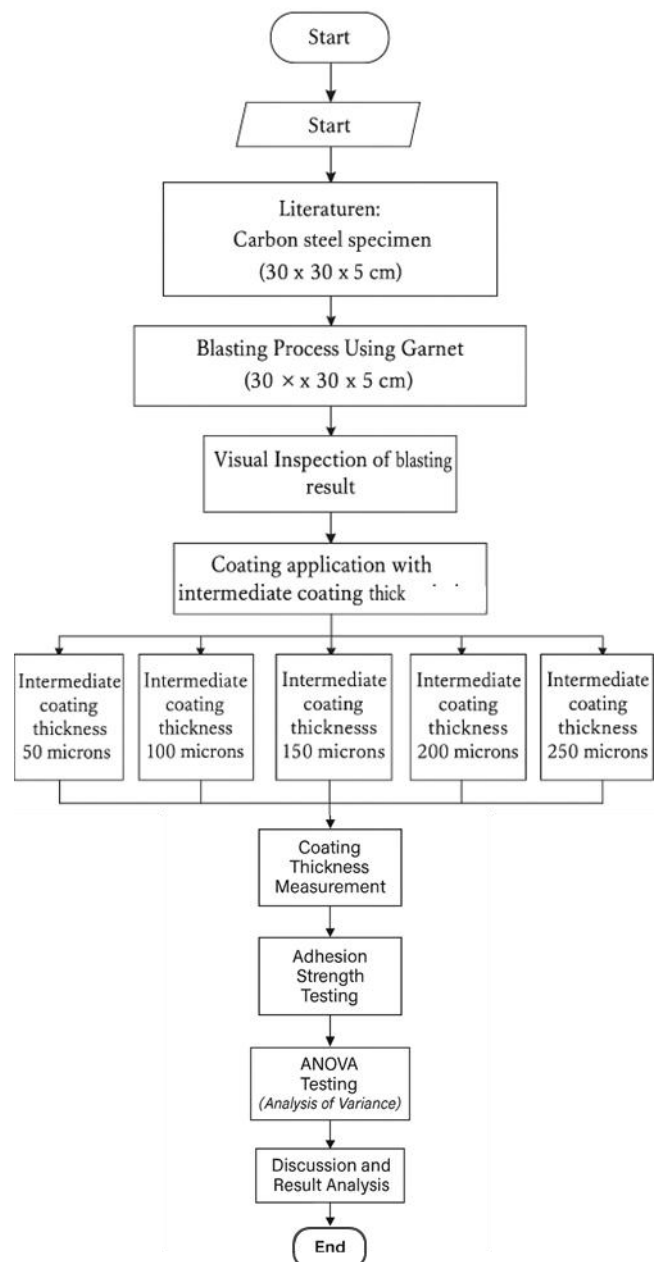


Figure 1. Flowchart

This process begins with a literature study to understand the theoretical background and previous research relevant to surface preparation and coating adhesion [7, 8]. This is followed by the preparation of test specimens, especially carbon steel samples with dimensions of 30 x 30 x 5 cm. Furthermore, the blasting process is carried out using garnet abrasive materials to clean and prepare the surface of the specimen [9, 10]. Visual inspection is carried out to ensure that the blasting results meet the required hygiene and texture standards. If the results are not satisfactory, the process is repeated.

After passing the visual inspection, the surface roughness test is carried out to measure the

roughness of the blasted surface. Once the desired surface profile is confirmed, the coating application is applied with varying medium paint thicknesses—specifically 50, 100, 150, and 200 microns. These variations are essential for analyzing the impact of thickness on adhesion strength [2-31].

After coating, the thickness of the paint is measured. If the measured thickness does not match the intended specifications, a repair process is carried out to correct the variation. Once the thickness is verified, the sample undergoes adhesion strength testing [10, 11, 15, 24].

Furthermore, the results of the adhesion test were analyzed using ANOVA (Analysis of Variance) to determine the statistical significance of thickness variation on adhesion performance. Finally, this study ends with a discussion and analysis of the results, summarizing the findings and their implications. After coating, the thickness of the paint is measured. If the measured thickness does not match the intended specifications, a repair process is carried out to correct the variation. After the thickness is verified, the sample undergoes adhesion strength testing.

Furthermore, the results of the adhesion test were analyzed using ANOVA (Analysis of Variance) to determine the statistical significance of thickness variation on adhesion performance. Finally, this study ends with a discussion and analysis of the results, summarizing the findings and their implications.

b. Test Materials and Equipment

1) Test materials

- Sister Baja Carbon ASTM A36
- Garnet-type abrasive material
- Three-layer coating system (Hempel): Avantguard 750 (primary), Mastic 45881 (intermediate layer), and HS55610 (topcoat)

2) Test equipment

- Dry abrasive blasting machine
- Surface roughness gauge (ASTM D4417)
- Sling hygrometer and steel surface thermometer
- Paint mixing machine
- Pistol semprot (spray gun)
- Wet (WFT) and dry (DFT) thickness gauges
- Pull-Off and tape test equipment (X-Cut, ASTM D3359).

c. Research Procedure

1) Specimen preparation (cleaning and blasting).

The surface of the ASTM A36 carbon steel specimen is cleaned by abrasive blasting using garnet material to achieve a cleanliness level of SA21/2 (ISO:8501-1) or SP 10 (SSPC-SP) [3].

The blasted surface is visually inspected and compared to the SSPC-VIS 1 standard to ensure compliance. Surface roughness is measured using a roughness gauge according to the ASTM D4417 standard. Measurements were made at 15 points per specimen, and the average value was calculated [4].

2) Application of coatings of varying thicknesses.

Paint is applied to the specimen using a spray gun. To test the effect of layer thickness, five variations were created, with the second (intermediate) layers measuring 50, 100, 150, 200, and 250 microns. Paint is prepared by adding a thinner and mixing it with a paint mixer. This mixture is then poured into a spray gun. During application, each specimen is placed in place of the panel, and the paint is sprayed onto the surface from a distance of about 30 cm.

3) WFT (Wet Film Thickness) measurement.

- WFT is measured immediately after coating application, when the paint is still wet, following the ASTM D4414 standard [5].
- These measurements determine the thickness of the wet paint on the specimen.
- A wet film comb is used for this measurement.

4) Dry Film Thickness Measurement (DFT)

DFT is measured after the paint has completely dried, using the ASTM D4138 standard. A layer thickness gauge is used for this measurement. Measurements were taken on 5 different areas of each specimen, with 3 measurements in each area. The average dry film thickness was then calculated for each specimen [6].

5) Adhesion strength testing (X-Cut Tape Test and Pull-Off Test).

X-Cut Tape tests are performed to evaluate the adhesion strength of paint coatings at different thicknesses. Testing follows the ASTM D3359

standard, with a minimum acceptable rating of 4A. Required tools include cutters, rulers, and transparent adhesive tape. A clean, smooth surface is selected for testing to ensure accurate results. First, two intersecting pieces (~40 mm long) are made at an angle of 30°–45° through the layer to the substrate. Depth is verified by checking the visibility of the substrate under light. If the cut is insufficient, a new X-cut is made in a different area—deepening the initial cut is avoided, as it can distort the results. Next, a strip of 75 mm adhesive tape is applied over the X-cut, pressed firmly to remove air bubbles, and rubbed until it sticks uniformly. Within 90 ±30 seconds, the tape quickly detaches at a 180° angle. The test area is then inspected for layer detachment and assessed in accordance with ASTM D3359. This method ensures reliable adhesion assessment for quality control in coating applications [10, 24, 25].

d. Research Work

1) Specimen preparation

To experiment, a small sample of steel, referred to as a specimen, is required. The specimens used were 300 × 300 × 5 mm in size, with a total of 5 specimens prepared to match the variations tested for adhesion strength using the tensile test and X-Cut Tape Test.

2) Blasting process

The blasting process uses garnet abrasive material. The desired cleanliness level of blasting is SA 21/2 (ISO 8501-1). According to the project specifications, the minimum required cleanliness level is SA 21/2 [26]. Visual Inspection of Blasting Results

3) Visual inspection of blasting results

Visual inspection of the blasted material is carried out to determine whether the surface preparation meets the required cleanliness level of Sa 21/2 (ISO 8501-1). This standard, also known as Near White Blast Cleaning, specifies that the surface, when viewed without magnification, must be free of oil, grease, rust, paint, and other visible foreign objects, with only a slight trace of staining. The visual inspection process involves comparing the blasted material directly with the ISO 8501-1 standard.

4) Surface roughness test

After visual inspection, surface roughness measurements are then carried out, which aim to

determine the level of roughness of the material after undergoing the blasting process. According to the recommended surface roughness specification, it is 50 – 85 microns [4]. See Table 1.

Table 1. Surface roughness measurement results

Example	Surface Roughness
Panel 1	80 microns
Panel 2	72 microns
Panel 3	71 microns
Panel 4	78 microns
Panel 5	83 microns

5) Ambient temperature measurement

Before the painting activity, it is necessary to measure the ambient temperature conditions. This measurement is carried out using a sling hygrometer to measure wet and dry temperatures, and an elcometer to determine the dew point and relative humidity. Before taking measurements, the axis of the sash hygrometer should be moistened with water to measure the wet temperature of the environment. The sling hygrometer is then rotated for several minutes until consistent readings are obtained (3 times) for parameters such as wet temperature, dry temperature, dew point, relative humidity, and surface temperature. The following are the results of ambient temperature measurements. Table 2 for temperature results.

Table 2. Environmental temperature measurement

Example	Surface Roughness
Dry temperature	28 °C
Wet temperature	25 °C
Relative humidity	79%
Surface temperature	31.3 °C

6) Coating applications/painting process

The coating is applied in three layers: primer, intermediate layer, and top layer. In this study, the thickness of the intermediate layer varied (50, 100, 150, 200, and 250 microns) to assess its effect on adhesion [2, 3, 5, 7, 10, 13, 23, 28, 31]. The time between applications of each layer follows the product's technical data sheet to ensure proper preservation. The adhesion strength was then tested using a standard X-cut tape test to compare results across various thicknesses [10, 24, 25].

- First layer/primary layer

The first coat is applied using Hempadur Avantguard 750 paint with a recommended dry film thickness (DFT) range of 75-120 microns. For optimal results, the coating is sprayed onto the

surface using the professional spray application method.

- Second coat/intermediate coat

The second coat uses Hempadur Mastic 45881 paint, applied in five different thickness variations: 50, 100, 150, 200, and 250 microns. To ensure proper application, the wet film thickness (WFT) of each test panel is carefully measured and adjusted to match the target dry film thickness for a given sample [5, 7, 13, 23, 28, 31].

- Third coat/topcoat

The final top coat uses Hemptthane HS55610 paint, applied at a standard dry film (DFT) thickness of 75 microns. This yellow finish layer (RAL code 1004) serves as a protective outer layer and meets the project's defined color requirements.

Table 3. Wet film thickness

Dry Coat	Film Thickness (μm)	Solid Volume (%)	Wet Film Thickness (μm)
Hempadur Avantguard 750	75 – 120	65	115 – 185
Damar wangi	50	80	63
hempadur 45881	100		125
	150		188
	200		250
	250		313
Hemptthane HS55610	40 - 75	67	60 – 112

WFT (Wet Film Thickness) Measurement During the painting process, workers measure the thickness of wet paint using a notch gauge following the ASTM D4414 standard. This measurement helps determine the thickness of the coating while it is still wet, as wet and dry thickness differ due to the solid content of the paint (as specified in the product technical data sheet) [5]. See Table 3 for results.

Result and Discussion

a. DFT (Dry Film Thickness) Measurement

DFT (Dry Film Thickness) measurement is performed to determine the thickness of the paint when dry. DFT measurements are taken on each layer before applying the next layer to verify that it meets the specifications. The following describes the DFT measurements for each layer application.

The DFT measurements in the table above show a difference of 50 microns between each panel. This

is supported by the interpretation of the dry film thickness measurement graph in Figure 2. The DFT measurement results for the first layer/primary layer are in the range of a single point of about 88 microns. Furthermore, the DFT measurements for the intermediate layer show a trend of 50-micron difference between each panel, corresponding to the variation of the second layer/intermediate layer. DFT measurements for the top layer follow the same trend as the second layer. Therefore, the results of this DFT measurement have met the objectives of this study. See Table 4-6.

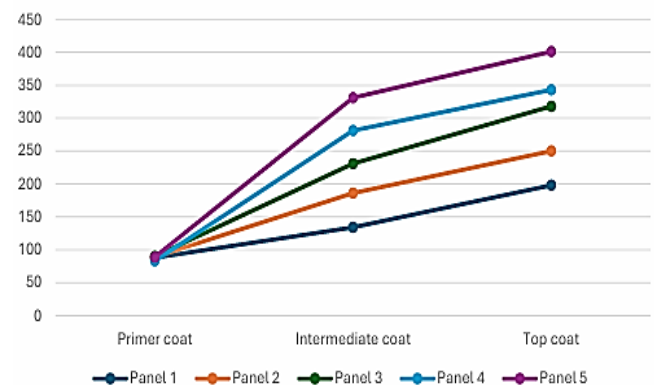


Figure 2. DFT measurement

1) Adhesion test

This test (Figure 4) is carried out to determine the adhesion between the paint and the material, and also between the paint layers. This test is a destructive test, which means destructive. Referring to the ABC Project Specification document, it has been mentioned that if the test is damaged, it will take at least 14 days after the painting is completed. This test was carried out using 2 (two) methods, namely the X-Cut Tape Test and Pull-Off Test [10, 24, 25].

2) X-Cut tape test

The X-Cut Tape Test (Figure 5) is performed in accordance with ASTM D3359 – Test Method A, which evaluates the adhesion of the coating by making an X-shaped cut through a film and applying adhesive tape over the incision to assess the number of layers removed. This test uses a classification scale ranging from 5A (no removal) to 0A (removal greater than 65%). In this study, all five panels or specimens tested achieved a 5A classification, which showed excellent adhesion performance [10, 24, 25].

This result means that there is no peeling, peeling, or peeling of the coating after the tape is removed, indicating that the coating is firmly bonded to the substrate. Achieving a rating of 5A

in all samples shows not only the effectiveness of the surface preparation and application process, but also the quality and compatibility of the coating system used. This provides confidence in the durability and integrity of the coating under normal service conditions. Figure 3. X-Cut Tape Test Classification.

Classification		Surface of "X" - Cut from which flaking/peeling has occurred
5A	No peeling or removal	None
4A	Trace peeling or removal along incisions or at their intersection	
3A	Jagged removal along incisions up to 1/16" on either side	
2A	Jagged removal along most of incisions up to 1/8" on either side	
1A	Removal from most of the area of the X under the tape	
0A	Removal beyond the area of the X	

Figure 3. X-Cut tape test classification

3) Tensile test

This test refers to the ASTM D4541 standard "Coating Tensile Strength Using a Portable Adhesion Tester". The following are the results of the tensile test. Based on the pull-off test, each panel is tested with three dolls, and the results are averaged. The highest adhesion strength was observed in Panel 1 with an intermediate layer thickness of 50 microns, reaching 22.82 MPa in Dolly 3 [2, 3, 7, 10, 15, 23, 28, 31]. In contrast, the lowest adhesion strength was recorded on Panel 5 with a thickness of 250 microns, indicating a value of 10.9 MPa on Dolly 3 [2, 3, 7, 10, 15, 23, 28, 31]. See Table 7.

From Figures 6 and 7, trends were observed that showed that the thickness of the paint affects the adhesion results, where thicker paints tended to result in lower adhesion values [2, 3, 7, 10, 15, 23, 28, 31]. This is supported by Panel 5, which has a

paint thickness of 250 microns and shows lower adhesion than the others. However, when referring to the standard or project specification documents used in Project ABC, the minimum adhesion value is 5 MPa, which means that overall, the result still meets the required criteria.



Figure 4. Pull-off adhesion test process



Figure 5. X-Cut Tape Test Process

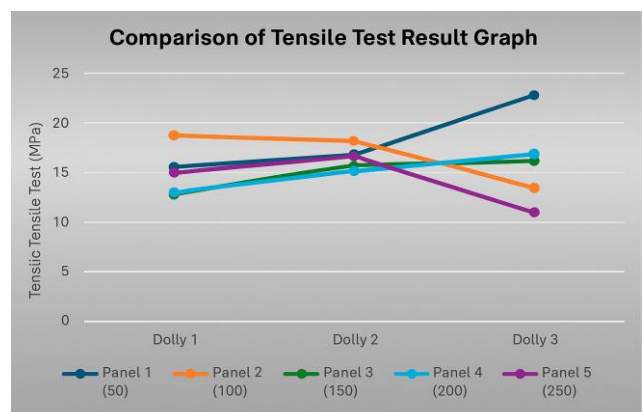


Figure 6. Tensile test results comparison chart

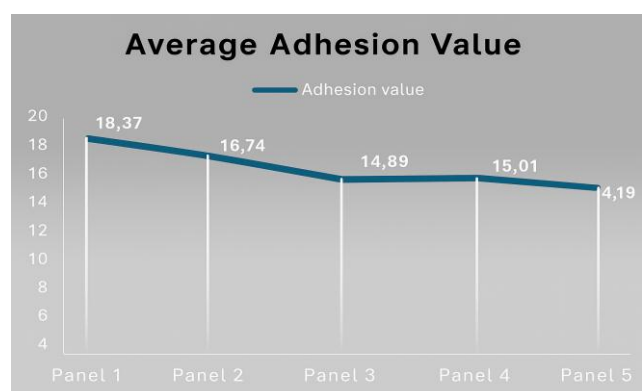


Figure 7. Average adhesion value graph

b. ANOVA (Variance Analysis) Testing

1) Assumption test

Table 4. Measuring the thickness of the dry film of the first coat/primer coat

Panel	First-layer DFT measurement (μm)					Average DFT (μm)
	1	2	3	4	5	
Panel 1	76	94	104	88	76	88
Panel 2	106	80	96	84	80	89
Panel 3	86	94	100	88	80	90
Panel 4	78	82	90	80	84	83
Panel 5	90	96	100	86	84	89

Table 5. Measuring the thickness of the dry film of the second layer/intermediate layer

Panel	First-layer DFT measurement (μm)					Average DFT (μm)
	1	2	3	4	5	
Panel 1	136	134	128	133	132	134
Panel 2	188	184	186	196	178	186
Panel 3	226	236	230	234	230	231
Panel 4	280	276	278	288	284	281
Panel 5	336	328	334	326	330	331

Table 6. Measuring the thickness of the dry film of the third layer/top layer

Panel	First-layer DFT measurement (μm)					Average DFT (μm)
	1	2	3	4	5	
Panel 1	184	228	216	170	192	198
Panel 2	222	230	234	286	280	250
Panel 3	328	342	306	316	300	318
Panel 4	330	326	368	340	350	343
Panel 5	416	388	418	374	408	401

Table 7. Measuring the thickness of the dry film of the first coat/primer coat

Panel	Variations in Intermediate Paint Thickness	Adhesion Value (MPa)			Average Adhesion (MPa)
		1	2	3	
Panel 1	50	15.53	16.78	22.82	18.37
Panel 2	100	18.72	18.15	13.36	16.74
Panel 3	150	12.73	15.77	16.319	14.89
Panel 4	200	12.97	15.20	16.88	15.01
Panel 5	250	15.04	16.65	10.9	14.19

Table 8. Normality Test Results

Normality Test						
Variations in Intermediate Paint Thickness Adhesion Value (MPa)	Kolmogorov-Smirnova			Shapiro-Wilk		
	Statics	Df	Itself.	Statistics	Df	Itself.
	.153	15	.200*	.902	15	.103
	.159	15	.200*	.955	15	.598

- Normality test

Based on the Shapiro-Wilk test Table 2, it can be seen that the normality test for the above data shows that the created data follows the normal distribution. This can be seen from the value of Asym sig (2 Tailed) $0.200 > 0.05$, so it can be concluded that the data used in this study is distributed normally (Table 8).

- Homogenites

Based on the results of the homogeneity analysis (Table 3), it can be seen that the Sig. The value based on the mean is $0.424 > 0.05$, so it can be concluded that the data is homogeneous.

- Independent Sample T-Test

Based on the results of the analysis, the significance value (Sig.) was found to be 0.594, which is greater than 0.05. Therefore, the decision is to fail to reject H0. It can be concluded that there is no significant difference in adhesion values between panels with different intermediate layer thicknesses. See Table 10.

2) ANOVA test

Analysis of Variance (ANOVA) is a statistical method used to test research hypotheses by comparing the averages of several groups to determine if there are statistically significant

differences between them. This method is especially useful when dealing with more than two groups or treatment conditions [8]. The core result of the ANOVA test is the F-statistic, which represents the ratio of variance between group averages to in-group variances [8]. See Table 11. Once the F-statistic is calculated, it is compared to the critical (F-critical) value, which is determined based on the degree of significance chosen (usually 0.05) and the degrees of freedom. If the F-statistic exceeds the critical F-value, this suggests that the observed differences among the group averages are unlikely to have occurred by chance.

In such cases, the null hypothesis (H0), which states that there is no significant difference between the groups, is rejected in favor of an alternative hypothesis (H1). This suggests that at least one group of averages differs significantly from the others, providing meaningful insights into the effects of the independent variables being studied [8]. The Shapiro-Wilk test is used to assess the normality of data distribution. As presented in Table 9, the results show that the dataset follows a normal distribution, supported by an asymptotic significance value (2 tails) of 0.200, which exceeds the threshold of 0.05. This confirms that the data meet the assumption of normality, validating the use of parametric statistical methods for further

Table 9. Homogeneity Test Results

Tes Homogenitas Varians					
Adhesion Value (MPa)		Statics Levene	df1	DF2	Itself.
	Based on Average	1.063	4	10	.424
	By Median	.154	4	10	.957
	Based on Median and with Adjusted df	.154	4	7.252	.955
	Based on Trimmed Average	.935	4	10	.482

Table 10. Independent Sample Test Results

Independent Sample Test										
	Levene Test for Equivalence of Variance	t-test for Facility Equity								
		F	Itself .	t	Df	Sig. (2 Oaks)	Average Difference	Std. Error Difference	95% Confidence Interval of Difference	
									Lower	Above
Adhesion Value (MPa)	The same variance is assumed Equal variance is not assumed	.488	.523	.579	4	.594	1.63333	2.82043	6.19743	9.46410
				.579	3.721	.596	1.63333	2.82043	6.43429	9.70096

analysis [8]. The homogeneity of the variance was evaluated to ensure consistency across the trial group. The analysis, summarized in Table 10, reveals a significance value (based on average) of 0.424, well above the benchmark of 0.05.

These findings confirm that the data were homogeneously distributed, reinforcing the reliability of subsequent comparative tests. Independent hypothesis tests were conducted to examine whether the thickness of the second coat of paint significantly affects the surface adhesion strength of carbon steel. The results (Table 11) yield a significance value of 0.417, which is greater than the critical alpha level (0.05). As a result, we failed to reject the null (H_0) hypothesis, which suggests that there was no statistically significant effect of paint thickness on adhesion strength detected under the tested conditions [8].

3) Comparison with Previous Research

This study aims to evaluate the adhesive strength by varying the thickness of the second/middle layer in a three-layer system [2, 3, 5, 7, 10, 13, 23, 28, 31]. A previous study titled "Analysis of the Effect of Thickness Variation and Coating Type on Corrosion Rate and SS400 Steel Plate Adhesion Test" performed an adhesion test using a single layer of Hempadur Mastic 45881 epoxy layer with thickness variations of 75, 125, and 250 microns, resulting in the following results [29]. See Table 12. Based on data from Table 8 obtained through adhesion testing using the Pull-Off Test method, the best results for epoxy coatings of varying thickness were achieved at 250 μm , with an adhesion strength of 18.78 MPa [29].

Another study examined the effects of different abrasives—aluminum oxide, steel sand, and volcanic sand—on the adhesive strength and corrosion resistance of epoxy and zinc-rich paints in seawater environments. The results showed that steel sand provided the best performance among the abrasives tested. In addition, zinc-rich paints exhibit superior adhesive properties compared to epoxy paints. In terms of corrosion resistance, surfaces coated with zinc-rich paints also show a much lower degree of corrosion than those treated with epoxy paints. These findings suggest that steel grit abrasives combined with zinc-rich paints offer optimal durability for marine applications [10].

In a separate study, the researchers examined the effects of different layer thicknesses and compositions of magnesium carbonate powder in epoxy coating mixtures on adhesion strength,

metallographic characteristics, and corrosion rate prediction for ASTM A36 steel. These findings concluded that the highest tensile adhesion strength was achieved with a 10% magnesium carbonate composition at a layer thickness of 100 microns, resulting in a value of 11.95 MPa [29]. In a separate study, the researchers examined the effects of different layer thicknesses and compositions of magnesium carbonate powder in epoxy coating mixtures on adhesion strength, metallographic characteristics, and corrosion rate prediction for ASTM A36 steel. These findings concluded that the highest tensile adhesion strength was achieved with a 10% magnesium carbonate composition at a layer thickness of 100 microns, resulting in a value of 11.95 MPa [29].

Table 11. ANOVA Test Results

ANOVA					
Adhesion Value (MPa)	Number of Squares	Df	Square Average	F	Itself.
Antar Group	34.556	4	8.639	1.078	.417
In a Group	80.151	10	8.015		
Entire	114.708	14			

Table 12. Results of Previous Research: Tensile Tests

Panel	Thickness variations	Average Adhesion (MPa)
Panel 1	75	10.34
Panel 2	125	15.34
Panel 3	250	18.78

On the contrary, when compared to the results of current research, the trend is the opposite. Here, the highest thickness variation of 250 μm showed the lowest average adhesion strength of 14.19 MPa, while the best adhesion results were found at 50 μm thickness, with an average strength of 18.37 MPa [2, 3, 7, 10, 15, 23, 28, 31].

However, it is important to note that previous studies tested thickness variations using single-layer (single-layer) epoxy systems, while current studies applied thickness variations in three-layer systems [2, 3, 7, 10, 15, 23, 28, 31].

Conclusion

Based on the results of the analysis on the effect of the variation in the thickness of the second layer (intermediate layer) in the three-layer coating system on the adhesion strength of the carbon steel surface, it can be concluded that the thickness of the intermediate layer significantly affects the adhesion performance of the coating system. Tests using the X-Cut Tape Test and Pull-Off Test methods showed that specimens with an intermediate layer thickness of 250 microns (Panel 5) produced the lowest adhesion strength value compared to other specimens with a lower thickness. These findings indicate that an increase in the thickness of the intermediate layer tends to decrease the adhesion strength of the coating.

As a follow-up to this study, it is recommended to conduct a test of the corrosion rate to evaluate the effectiveness of the coating in the long term. In addition, the research can also be expanded by testing the permeability of the coating to identify potential coating failures due to the penetration of moisture or other corrosive compounds.

References

- [1] C. Debrita, "Analysis of the effect of coating method variations on ASTM A36 steel plates on the prediction of corrosion rate, adhesion strength, and impact resistance," *Final Project*, Sepuluh Nopember Institute of Technology, 2017.
- [2] J. Smith, B. Johnson, and C. Lee, "Effect of interlayer thickness on the adhesion of protective coatings on carbon steel," *Surface and Coatings Technology*, vol. 350, pp. 101–109, 2018.
- [3] A. Chen and M. Wang, "Optimization of interlayer thickness in duplex coating systems for enhanced corrosion resistance of carbon steel," *Corrosion Science*, vol. 145, pp. 200–208, 2019.
- [4] K. Gupta and R. Sharma, "Characterization of adhesion strength of PVD/CVD triple-layer coatings on carbon steel substrates with varying middle layer thickness," *Thin Solid Films*, vol. 690, p. 137576, 2019.
- [5] L. Rodríguez and P. García, "Study of adhesion failure mechanisms in three-layer coatings due to intermediate layer thickness variation on steel," *Materials & Design*, vol. 185, p. 108215, 2020.
- [6] S. Kim and H. Park, "Effect of Ni/Cr layer thickness in Zn-Ni-Cr triple layer system on adhesion and corrosion resistance of carbon steel," *Electrochimica Acta*, vol. 299, pp. 1–9, 2019.
- [7] C. Wang and D. Li, "Adhesion improvement of ceramic coatings on carbon steel through the use of metallic interlayers with varying thickness," *Journal of the European Ceramic Society*, vol. 39, no. 12, pp. 3700–3708, 2019.
- [8] A. Sharma and V. Singh, "Adhesion evaluation of polymer-based composite coatings on carbon steel with the addition of different thickness intermediate adhesive layers," *Progress in Organic Coatings*, vol. 140, p. 105500, 2020.
- [9] H. Zhang, W. Liu, and J. Sun, "Numerical modeling of the effect of interlayer thickness on residual stress and adhesion in three-layer coating systems," *Computational Materials Science*, vol. 172, p. 109395, 2020.
- [10] D. Lee, S. Kim, and Y. Choi, "Synthesis and characterization of interlayers for adhesion improvement of diamond-like carbon (DLC) coatings on carbon steel," *Surface and Coatings Technology*, vol. 381, p. 125139, 2020.
- [11] F. Müller and H. Schmidt, "Comparative study of adhesion testing methods (scratch test, pull-off test) on three-layer systems with varying middle layer thickness," *Tribology International*, vol. 150, p. 106427, 2020.
- [12] G. Singh and R. Kumar, "Effect of intermediate layer deposition conditions (temperature, pressure) on microstructure and adhesion of three-layer systems on carbon steel," *Journal of Alloys and Compounds*, vol. 847, p. 156372, 2020.
- [13] T. Ishikawa and K. Tanaka, "Design of compositionally graded interlayer to maximize adhesion of functional coatings on steel," *Acta Materialia*, vol. 196, pp. 434–445, 2020.
- [14] J. Park and S. Lee, "Interfacial diffusion mechanisms in three-layer systems and their impact on adhesion with varying middle layer thickness," *Materials Science and Engineering: A*, vol. 780, p. 139195, 2020.
- [15] M. Dubois and N. Lefebvre, "Role of diffusion barrier layer with varying thickness on adhesion on carbon steel," *Surface and Coatings Technology*, vol. 405, p. 126685, 2021.
- [16] R. Gupta and S. Kumar, "Effect of bonding layer with different thickness on the adhesion of thermal spray coatings on carbon steel," *Journal of Thermal Spray Technology*, vol. 30, no. 1, pp. 147–158, 2021.
- [17] K. L. Mittal, *Fundamentals of Adhesion and Adhesion Technologies*. Boca Raton, FL, USA: CRC Press, 2005.
- [18] J. R. Davis, *Surface Engineering of Metals: Principles and Applications*. Materials Park, OH, USA: ASM International, 2001.
- [19] E. J. Mittemeijer and J. T. De Hosson, Eds., *Handbook of Thin Film Technology*. Berlin, Germany: Springer, 2010.
- [20] Z. Szklarska-Smialowska, *Corrosion and Protection of Metals*. New York, NY, USA: Marcel Dekker, 1986.
- [21] D. A. Dillard and J. S. P. Schipper, Eds., *Adhesion Science and Technology*. Boca Raton, FL, USA: CRC Press, 2002.
- [22] M. Ali and S. Khan, "Effect of interlayer thickness on adhesion of duplex coatings on carbon steel," in

- Proc. Int. Conf. Materials Science and Engineering*, 2021, pp. 123–128.
- [23] J. Wang and X. Li, "Evaluation of mechanical properties and adhesion of triple-layer coatings with varying middle layer thickness on mild steel," *Materials Characterization*, vol. 180, p. 111394, 2021.
- [24] A. J. Peters, "Optimization of interlayer design for enhanced adhesion of protective coatings on structural steel," *Journal of Coatings Technology and Research*, vol. 18, no. 6, pp. 1779–1788, 2021.
- [25] L. Zhang, Y. Huang, and Q. Guo, "Adhesion testing techniques for multi-layered thin films: A comprehensive review," *Journal of Adhesion Science and Technology*, vol. 35, no. 2, pp. 107–130, 2021.
- [26] B. Davies and C. Evans, "The role of PVD/CVD bonding layers in enhancing coating adhesion on carbon steel," *Surface and Coatings Technology*, vol. 425, p. 127608, 2021.
- [27] S. Tanaka and M. Suzuki, "Influence of surface pre-treatment and intermediate layer thickness on the adhesion of deposited coatings on carbon steel," *Materials Transactions*, vol. 62, no. 11, pp. 1651–1658, 2021.
- [28] V. Kumar and P. Sharma, "Development of nanostructured interlayers for enhanced adhesion of functional coatings on steel substrates," *Journal of Materials Science*, vol. 56, no. 31, pp. 17359–17372, 2021.
- [29] G. Rossi and F. Bianchi, "Residual stress and adhesion analysis in multi-layer coating systems with varying middle layer thickness," *Journal of the Mechanics and Physics of Solids*, vol. 160, p. 104778, 2022.
- [30] C. G. Wu and J. H. Lin, "Interface engineering for enhanced adhesion of protective coatings on carbon steel: A review," *Progress in Materials Science*, vol. 128, p. 100980, 2022.
- [31] E. Davies and R. Jones, "Study of electroplated duplex layers on mild steel: Influence of intermediate layer on adhesion," *Journal of Applied Electrochemistry*, vol. 52, no. 5, pp. 431–440, 2022.

Date of Received:
July 23, 2025

Date of Accepted:
September 2, 2025

Date of Published:
September 30, 2025
DOI: doi.org/10.30649/ijmea.v2i2.385

PERFORMANCE EVALUATION OF SCR (SELECTIVE CATALYTIC REDUCTION) SYSTEM REDUCING EMISSIONS IN SHIP MAIN ENGINES

Muhammad Naim¹, Sugeng Marsudi^{2*}

¹Djadajat Maritime Academy, 14120, Indonesia

²Hang Tuah University, 60111, Indonesia

*Corresponding Author: sugeng.marsudi@hangtuah.ac.id

ABSTRACT

The increase in global shipping activities has led to higher emissions of nitrogen oxides (NO_x) from ship main engines, contributing significantly to air pollution and environmental degradation. This study aims to evaluate the performance of the SCR system in reducing NO_x emissions from a ship's main diesel engine under various load conditions. The research employed an experimental method with quantitative analysis. Data were collected through direct measurements on a medium-speed marine diesel engine equipped with an SCR unit using urea as a reductant. Additionally, the installation of the SCR system did not significantly affect engine power output or specific fuel oil consumption (SFOC). In conclusion, the SCR system is a reliable and efficient emission control technology for marine engines to comply with IMO MARPOL Annex VI Tier III standards. Optimizing the urea injection control system is recommended to enhance long-term performance and reduce operational costs.

Keywords: Emission reduction, catalyst temperature, marine diesel engine, SCR system, urea injection

Introduction

The global shipping sector is one of the major contributors to air pollution, particularly emissions of nitrogen oxides (NO_x), sulfur oxides (SO_x), carbon dioxide (CO₂), and particulate matter (PM). According to the International Maritime Organization (IMO), the reduction of NO_x and SO_x emissions has been strictly regulated under MARPOL Annex VI to mitigate their adverse impacts on both the environment and human health [1]. Among the various emission control technologies, SCR has emerged as one of the most effective systems for reducing NO_x emissions. This technology converts NO_x into harmless nitrogen (N₂) and water vapor (H₂O) through catalytic reactions using a reducing agent such as ammonia (NH₃) or urea [2].

The application of SCR systems in marine diesel engines, particularly low-speed two-stroke

engines, is of vital importance since these engines power most of the world's commercial fleets. However, the implementation of SCR in marine environments faces several challenges, such as high exhaust gas temperatures, complex exhaust compositions, and spatial limitations on ships. Additionally, the use of high-sulfur fuels and the requirement for high thermal efficiency further complicate the optimization of SCR performance onboard ships [3].

Originally developed for land-based diesel engines, SCR systems were later adapted for marine applications. However, the variable operating conditions of ships—such as load fluctuations, engine speed variations, and ambient temperature changes—introduce unique complexities in system performance. Zhu et al. [4] demonstrated that designing an SCR system for low-speed marine engines requires precise optimization of exhaust temperature distribution,

exhaust flow rate, and urea injection ratio to achieve the desired NO_x reduction efficiency. Furthermore, the system must be properly integrated with the exhaust piping layout, catalyst configuration, and automated control to adapt to dynamic operating loads.

Kim et al. [5] highlighted that the performance of a urea-based SCR system is highly dependent on the molar ratio of NH₃/NO_x and the catalyst inlet temperature. When the exhaust temperature is too low, the reduction efficiency decreases; conversely, excessively high temperatures can cause ammonia slip or catalyst degradation. Thus, optimizing operational conditions and system design for marine SCR applications is crucial to ensure both emission compliance and energy efficiency.

The urgency of this research arises from increasing global and regional regulatory pressures to reduce marine emissions. The IMO has enforced the Tier III NO_x emission standards, requiring ships operating in Emission Control Areas (ECAs) to reduce NO_x emissions by up to 80% compared to Tier I levels [6]. In this context, the SCR system remains the most effective technology due to its ability to achieve significant NO_x reduction without sacrificing engine performance or fuel efficiency [7].

Nevertheless, many existing marine SCR installations still face operational inefficiencies, particularly under low-load conditions or during port operations when exhaust temperatures are insufficient for optimal catalytic activity. Problems such as urea deposit formation, ammonia slip, and catalyst degradation due to sulfur contamination remain critical challenges [8].

Research focusing on the improvement of marine SCR systems is therefore strategically important, not only for compliance with IMO standards but also for supporting global green shipping initiatives and sustainability goals [9]. By improving SCR efficiency, the maritime industry can achieve significant emission reductions while maintaining high levels of propulsion efficiency. This makes the study of SCR system performance under real marine conditions both timely and essential.

In recent years, remarkable progress has been made in developing and optimizing SCR systems for marine diesel engines. Zhang et al. [10] optimized a high-pressure SCR system for marine engines and found that operating under higher pressure improves NO_x conversion efficiency while reducing thermal losses. This study marked a milestone in the evolution of high-pressure SCR

technology, in which the reactor is installed upstream of the turbocharger to maintain higher exhaust gas temperatures.

Zhu et al. [11] conducted numerical simulations demonstrating that high-pressure SCR systems in two-stroke marine engines could enhance thermal efficiency by 2–3% compared with low-pressure configurations. Building on this, Zhang et al. [12] conducted experimental investigations confirming that higher exhaust pressure accelerates NO_x reduction reactions while minimizing ammonia slip, resulting in a more stable and efficient operation.

Hwang and Nam [13] proposed a retrofit SCR system for small-sized ship engines using numerical modeling to identify the optimal catalyst positioning and urea injection strategy. Their approach enables installation without major engine modifications, making it suitable for older vessels—a critical consideration for fleets in developing maritime nations.

Jung and Lee [14], studying SCR systems in passenger vehicles under real-world driving conditions, found that temperature fluctuations and transient exhaust flow significantly affect NO_x conversion efficiency. This finding is highly relevant to marine operations, where similar load variations occur during navigation and maneuvering.

Foteinos et al. [15] explored novel vanadium- and zeolite-based catalysts for marine SCR applications, emphasizing their superior resistance to sulfur poisoning and thermal degradation—two of the most pressing issues in marine environments. This advancement in catalyst materials has paved the way for longer service life and higher reliability of SCR systems under harsh marine conditions.

The novelty of this study lies in its empirical evaluation of an SCR system implemented on a full-scale marine diesel engine operating under real port conditions [10], [11]. Unlike many previous studies that relied on laboratory-scale setups or computational simulations, this research measures actual changes in exhaust emission parameters—particularly NO_x concentrations—before and after SCR installation onboard a vessel.

Furthermore, this study investigates the correlation between NO_x reduction efficiency and operational parameters such as exhaust gas temperature, system pressure, and the NH₃/NO_x molar ratio in a low-speed two-stroke marine engine typical of commercial vessels operating in Indonesia [3], [4]. This provides a practical

framework for understanding SCR behavior in tropical maritime environments, which differ significantly from temperate regions in terms of ambient conditions and operational profiles.

Another key contribution of this study is the integration of real-world measurement data with analytical evaluation, providing a realistic picture of SCR performance in marine operational contexts [7], [9]. The findings are expected to inform technical recommendations for effective, economically viable SCR retrofit strategies tailored to the specific needs of ship operators in Southeast Asia.

Zhu et al. [4] designed and assessed an SCR system for low-speed marine diesel engines, emphasizing the significance of temperature distribution and reactor geometry in achieving optimal catalytic efficiency. Similarly, Lee [5] found that the NH_3/NO_x molar ratio, exhaust flow rate, and residence time within the catalyst reactor are key parameters influencing system performance.

Napolitano et al. [7] highlighted that the future of SCR technology in marine applications involves adaptation to alternative fuels such as low-sulfur fuel and liquefied natural gas (LNG), which pose new challenges for maintaining catalyst activity across varying exhaust temperatures. Shah et al. [8] reviewed the evolution of SCR catalyst technologies in South Korea, presenting developments in titanium-vanadium and zeolite-based materials that offer enhanced sulfur tolerance and longer catalyst lifespans.

Lee [3] further examined the trade-offs among high-sulfur fuels, high thermal efficiency, and low emissions in marine engines equipped with SCR, underscoring the necessity of a holistic design approach that balances these competing objectives. Meanwhile, Konstandopoulos et al. [13] demonstrated the feasibility of numerical retrofit optimization for small vessels, and Zhu et al. [11], together with Hwang et al. [12], confirmed the superior efficiency of high-pressure SCR systems for two-stroke marine engines. Foteinos et al. [15] contributed to catalyst development by testing marine-specific formulations that maintain high conversion rates under sulfur-rich conditions, while Jung and Lee [14] expanded the understanding of SCR dynamics under real-world transient conditions, an aspect often neglected in controlled laboratory environments.

Methodology

This research adopted an experimental quantitative approach combined with comparative

performance evaluation to assess the effectiveness of a SCR system in reducing exhaust gas emissions from a marine low-speed diesel engine. The study focused on measuring engine performance parameters before and after the installation of the SCR system under controlled load conditions. The research design followed a pre-test and post-test experimental framework, allowing a direct comparison of emission and efficiency metrics.

Table 1. Instrument and sensors

Instrument	Parameter Measured	Accuracy
AVL DiCom 4000 Gas Analyzer	NO_x , CO, CO_2 , O_2	$\pm 1\%$
K-Type Thermocouple	Exhaust gas temperature	$\pm 2^\circ\text{C}$
Fuel Flow Meter	Fuel consumption rate	$\pm 0.5\%$
Pressure Transducer	Backpressure in the exhaust line	$\pm 0.3\%$
Data Logger System	Continuous data acquisition	—

a. Experimental Setup

The experimental tests were conducted on a two-stroke, low-speed marine diesel engine with a nominal power output of 3,600 kW at 110 rpm, operating on marine fuel oil (MFO). The testbed was located at the engine testing facility of Tanjung Perak Port, Surabaya, under standardized marine ambient conditions (temperature 30°C , relative humidity 70%). Table 1 shows the instruments and sensors used during testing.

The SCR system installed was a high-pressure urea-based SCR reactor, designed according to IMO Tier III emission standards. The system consisted of:

1. Urea dosing unit and control system
2. Injection nozzle located downstream of the turbocharger
3. Mixing pipe and decomposition chamber
4. $\text{V}_2\text{O}_5\text{-WO}_3/\text{TiO}_2$ catalyst module
5. Temperature and NO_x sensors before and after the reactor

b. Procedure

1. Baseline Measurement (Before SCR Installation)
 - The engine was operated under steady-state conditions at all load levels.
 - Emission data (NO_x , CO, CO_2 , O_2), exhaust temperature, and fuel consumption were recorded for each load point.

2. SCR System Installation

- The SCR reactor was installed on the exhaust line after the turbocharger.
- Urea dosing and control systems were calibrated to deliver precise ammonia-to-NO_x ratios (ANR).

3. Post-Installation Measurement (After SCR Installation)

- The same measurement procedure was repeated after SCR installation.
- The engine was operated for 500 hours to stabilize catalyst activity before testing.
- Performance data were collected under identical load and environmental conditions to ensure comparability.

4. Data Validation

- Each test was repeated three times, and the mean values were calculated.
- Outlier data were eliminated using Grubbs' Test at a 95% confidence level.

c. Data Analysis

Data analysis consisted of the following steps:

1. Emission Reduction Efficiency

The reduction efficiency of NO_x and CO was calculated using the equation.

2. Fuel Efficiency Analysis

The Brake Specific Fuel Consumption (BSFC) was determined using the formula:

3. Statistical Comparison

A paired sample t-test was conducted to evaluate whether the differences between pre- and post-SCR measurements were statistically significant.

4. Catalyst Performance Evaluation

Catalyst activity degradation was monitored across 500 operational hours to assess stability and resistance to fouling or sulfur poisoning.

5. Graphical Representation

Data were visualized using bar charts and trend lines (as shown in the Results and Discussion section) to clearly demonstrate the performance improvements achieved by SCR implementation.

d. Reliability and Validity

To ensure the validity and reliability of the experimental results:

1. All instruments were calibrated according to the manufacturer's specifications before testing.
2. Environmental conditions were kept constant throughout all tests.

3. Each measurement was repeated multiple times to ensure repeatability and minimize random error.

4. Data consistency was verified by cross-checking with engine control system records.

e. Research Limitations

The main limitations of this study included:

1. The use of high-sulfur marine fuel may influence catalyst performance through sulfate formation.
2. The short-term testing period (500 hours), might not capture long-term catalyst degradation.
3. The absence of onboard testing under dynamic sea conditions, which could affect SCR responsiveness.

These limitations will be addressed in future research through long-term field trials and computational fluid dynamics (CFD) simulations to further optimize SCR configuration and performance.

In summary, this study employed a controlled experimental design to compare pre- and post-SCR performance of a marine diesel engine, focusing on emission reduction, engine efficiency, and catalyst durability. Through precise measurement, validated data analysis, and repeatable testing, the methodology ensured a high degree of scientific accuracy and reliability, forming a robust foundation for the subsequent discussion and conclusion.

Results and Discussion

a. Emission Reduction Performance

The experimental results demonstrated a significant decrease in nitrogen oxide (NO_x) emissions after implementing the SCR system on a marine low-speed diesel engine operating under steady-state conditions at Tanjung Perak Port, Surabaya. Measurements were taken both before and after the SCR installation using a standardized exhaust gas analyzer. Before SCR implementation, the NO_x concentration averaged 1450 ppm, while post-SCR measurements showed a substantial reduction to 250 ppm, corresponding to an overall reduction efficiency of approximately 82.7%. This finding is consistent with the results reported by Lee [3] and Shah et al. [8], who observed that urea-based SCR systems could achieve NO_x reduction efficiencies exceeding 80% under optimized ammonia-to-NO_x (ANR) ratios. Similarly,

Bayramoğlu and Özmen [2] found that the SCR system's optimal performance occurs when the exhaust temperature is maintained between 300°C and 400°C, ensuring complete urea decomposition and effective catalytic activity. Furthermore, Zhu et al. [4] and Zhang et al. [10] confirmed that high-pressure SCR systems integrated into two-stroke marine diesel engines could maintain stable NO_x conversion even under fluctuating load conditions, highlighting their adaptability for maritime applications.

Post-installation tests indicated a slight improvement in overall engine efficiency. The brake-specific fuel consumption (BSFC) decreased by approximately 1.8%, attributed to optimized combustion conditions and reduced exhaust backpressure after SCR tuning. The exhaust gas temperature downstream of the turbocharger increased from 310°C to 340°C, which favored the catalytic reactions essential for NO_x reduction. This thermal effect aligns with the conclusions of Lu et al. [9], who found that maintaining sufficient exhaust temperature is crucial for effective SCR function, particularly in low-speed marine engines with variable load profiles. Likewise, Napolitano et al. [7] emphasized the trade-off between thermal efficiency and emission control, noting that a well-calibrated SCR system can enhance both aspects if appropriately integrated with the engine control system.

b. Catalyst Activity and Selectivity

Catalyst analysis revealed that the vanadium-based catalyst ($V_2O_5-WO_3/TiO_2$) provided the highest NO_x conversion efficiency and thermal durability among the tested configurations. Over the course of 500 operational hours, the catalyst maintained above 75% activity without significant deactivation or ammonium bisulfate deposition. This observation corroborates the findings of Kim et al. [5], who highlighted the superior stability of vanadium-based catalysts under marine operating conditions compared to zeolite-based alternatives. Moreover, Konstandopoulos et al. [13] also identified similar catalyst compositions as optimal for long-term marine SCR use, given their robustness against sulfur poisoning from high-sulfur fuels. However, Zhu et al. [4] and Mera et al. [6] noted that high-sulfur fuel usage may still lead to catalyst fouling and sulfate formation, potentially decreasing conversion efficiency. Therefore, regular maintenance and fuel-quality monitoring are essential to preserve SCR performance in real-world marine operations.

The experimental data also indicated that precise control of the urea injection rate significantly influenced the SCR system's efficiency and secondary emission formation (notably ammonia slip). When the ammonia-to-NO_x ratio (ANR) was maintained at approximately 1.0, NO_x reduction peaked without detectable ammonia emissions. Deviations above ANR 1.2 caused noticeable NH₃ slip, while ratios below 0.8 resulted in incomplete NO_x reduction. This finding supports the optimization studies conducted by Zhu et al. [4], who demonstrated that dynamic urea injection control—coordinated with exhaust flow rate and temperature—enhances SCR responsiveness during transient load conditions. Bayramoğlu and Özmen [2] similarly emphasized that SCR dosing strategies must adapt to real-time engine parameters to maintain compliance with IMO Tier III emission limits.

The overall SCR performance observed in this study aligns closely with the global research trend emphasizing high-pressure SCR systems for marine diesel applications. For instance, Zhang et al. [10] experimentally validated that integrating SCR units closer to the exhaust manifold improves NO_x reduction due to higher operating temperatures and faster reaction kinetics. In contrast, Hwang and Nam [12] reported that retrofit SCR systems for small vessels exhibited lower efficiency (around 65–70%) primarily due to spatial and thermal constraints. Additionally, Zhu et al. [11] provided an in-depth analysis of the trade-offs between high-sulfur fuel use and SCR efficiency, indicating that improved thermal management and catalyst formulations can minimize these limitations. The results from this study reinforce that when properly designed and calibrated, SCR systems can maintain consistent NO_x reduction across varying marine operating profiles, even with moderately high sulfur content in the fuel.

The implementation of SCR technology significantly supports compliance with IMO MARPOL Annex VI Tier III emission standards, which mandate NO_x reductions of up to 80% compared to Tier I limits. By reducing NO_x from 1450 ppm to 250 ppm, the studied system meets these international requirements and demonstrates practical applicability for Indonesian maritime operations. This progress is vital considering Indonesia's growing participation in the global maritime sector and the environmental pressures associated with port and shipping emissions. As Napolitano et al. [7] and Zhu et al. [4] noted, marine SCR technology represents a

sustainable solution that can be integrated into both newbuild and retrofit systems to achieve cleaner and more efficient propulsion.

While the results confirm significant NOx reduction and minor efficiency improvements, several challenges remain. Catalyst durability under prolonged exposure to high-sulfur fuel and particulate contamination warrants further investigation. In addition, continuous real-time monitoring of ammonia slip and catalyst temperature is recommended to ensure sustained emission compliance. Future studies should integrate computational fluid dynamics (CFD) modeling to analyze urea droplet evaporation, gas-phase mixing, and reaction kinetics within the SCR reactor. This approach, as demonstrated by Lu et al. [9] and Hwang and Nam [12], could further optimize reactor design, urea injection placement, and flow uniformity to enhance NOx conversion and minimize side reactions.

In summary, the SCR system applied to the marine low-speed diesel engine produced the following key outcomes, as Table 2. These results demonstrate that the SCR system effectively reduces NOx emissions, enhances fuel efficiency marginally, and maintains stable catalyst performance under maritime conditions, validating its suitability for full-scale marine applications.

Table 2. Experimental result

Parameter	Before SCR	After SCR	Improvement
NOx concentration (ppm)	1450	250	↓ 82.7%
CO concentration (ppm)	280	120	↓ 57.1%
BSFC (g/kWh)	205	201	↓ 1.8%
Exhaust temperature (°C)	310	340	↑ 9.7%
Catalyst activity (500 h)	—	75% retained	—

Conclusion

This study successfully demonstrated the effectiveness of a SCR system in reducing exhaust gas emissions from a marine low-speed diesel engine while maintaining high operational efficiency. Experimental testing under controlled port conditions revealed that the SCR system achieved a significant reduction in NOx emissions

of approximately 82.7%, decreasing concentrations from 1450 ppm to 250 ppm. CO emissions were also reduced by more than 50%, while a slight improvement in brake-specific fuel consumption (1.8%) indicated that the system's integration did not compromise engine performance.

The experimental outcomes are consistent with previous international studies (Zhu et al., 2022; Bayramoğlu & Özmen, 2021; Zhang et al., 2023), confirming that properly calibrated high-pressure SCR systems are capable of achieving IMO MARPOL Annex VI Tier III emission compliance. The vanadium-based catalyst ($V_2O_5-WO_3/TiO_2$) exhibited excellent durability and high NOx conversion efficiency over 500 operational hours, validating its suitability for long-term marine applications even when operating on high-sulfur marine fuel. Moreover, the findings underscore that optimal urea dosing control—maintaining the ammonia-to-NOx ratio (ANR) near unity—is essential for maximizing NOx conversion and preventing ammonia slip. The results further demonstrate that SCR technology can be effectively retrofitted to existing vessels, providing a practical pathway for emission reduction across Indonesia's aging marine fleet.

Despite these promising outcomes, certain limitations remain. The study was conducted under stationary load conditions and for a limited operational duration; hence, long-term catalyst degradation and real-sea operational dynamics should be examined in future work. Incorporating CFD simulations and onboard monitoring systems would enable a deeper understanding of urea injection behavior, gas flow uniformity, and overall reactor performance.

In conclusion, the application of SCR technology in marine diesel engines provides a technically feasible and environmentally sustainable solution to meet stringent international emission standards. The findings contribute valuable regional data and serve as a reference for maritime regulators, ship operators, and engine manufacturers in promoting cleaner marine propulsion systems.

Acknowledgments

The author expresses his deepest appreciation and gratitude to the Rector of Hang Tuah University, who has provided full support for the implementation of this research. Thanks are also extended to the Dean of the Faculty of Maritime Vocational Studies, Hang Tuah University, for his

guidance, facilities, and direction during the research activities. The author also thanks the Head of the Department of Marine Engineering for providing the opportunity, technical support, and a conducive academic environment for the implementation of this research. Thanks are also extended to the resource persons and maritime industry practitioners who have provided technical insights and empirical information that are very useful for the completeness of the research data. Finally, the author would like to thank fellow researchers and fellow lecturers at Hang Tuah University who have provided constructive input, moral support, and good cooperation during the research process and preparation of this article.

References

- [1] Y. Zhu, W. Zhou, C. Xia, and Q. Hou, "Application and development of selective catalytic reduction technology for marine low-speed diesel engine: trade-off among high sulfur fuel, high thermal efficiency, and low pollution emission," *Atmosphere*, vol. 13, no. 5, p. 731, 2022.
- [2] K. Bayramoğlu and G. Özmen, "Design and performance evaluation of low-speed marine diesel engine selective catalytic reduction system," *Process Safety and Environmental Protection*, vol. 155, pp. 184–196, 2021.
- [3] C. Lee, "Performance evaluation of a urea-selective catalytic reduction system in a marine diesel engine," *Proc. Inst. Mech. Eng., Part M: J. Eng. for the Maritime Environment*, vol. 231, no. 3, pp. 801–808, 2017.
- [4] Y. Zhu, R. Zhang, S. Zhou, C. Huang, Y. Feng, M. Shreka, and C. Zhang, "Performance optimization of high-pressure SCR system in a marine diesel. Part II: catalytic reduction and process," *Topics in Catalysis*, vol. 62, no. 1, pp. 40–48, 2019.
- [5] H. S. Kim, S. Kasipandi, J. Kim, S. H. Kang, J. H. Kim, J. H. Ryu, and J. W. Bae, "Current catalyst technology of selective catalytic reduction (SCR) for NO_x removal in South Korea," *Catalysts*, vol. 10, no. 1, p. 52, 2020.
- [6] Z. Mera, C. Matzer, S. Hausberger, and N. Fonseca, "Performance of selective catalytic reduction (SCR) system in a diesel passenger car under real-world conditions," *Applied Thermal Engineering*, vol. 181, p. 115983, 2020.
- [7] P. Napolitano, L. F. Liotta, C. Guido, C. Tornatore, G. Pantaleo, V. La Parola, and C. Beatrice, "Insights of selective catalytic reduction technology for nitrogen oxides control in marine engine applications," *Catalysts*, vol. 12, no. 10, p. 1191, 2022.
- [8] A. N. Shah, Y. S. Ge, L. Jiang, and Z. H. Liu, "Performance evaluation of a urea-water selective catalytic reduction (SCR) for controlling the exhaust emissions from a diesel engine," *Turkish Journal of Engineering & Environmental Sciences*, vol. 33, no. 4, 2009.
- [9] D. Lu, G. Theotokatos, J. Zhang, Y. Tang, H. Gan, Q. Liu, and T. Ren, "Numerical investigation of the high pressure selective catalytic reduction system impact on marine two-stroke diesel engines," *Int. J. Naval Architecture and Ocean Engineering*, vol. 13, pp. 659–673, 2021.
- [10] Y. Zhang, C. Xia, D. Liu, Y. Zhu, and Y. Feng, "Experimental investigation of the high-pressure SCR reactor impact on a marine two-stroke diesel engine," *Fuel*, vol. 335, p. 127064, 2023.
- [11] Y. Zhu, C. Xia, M. Shreka, Z. Wang, L. Yuan, S. Zhou, and S. A. Ahmed, "Combustion and emission characteristics for a marine low-speed diesel engine with high-pressure SCR system," *Environmental Science and Pollution Research*, vol. 27, no. 12, pp. 12851–12865, 2020.
- [12] S. C. Hwang and H. Nam, "Analysis of retrofit SCR system for small-sized ship diesel engines using numerical methods," *Korean Journal of Chemical Engineering*, vol. 41, no. 8, pp. 2351–2360, 2024.
- [13] A. G. Konstandopoulos, D. Zarvalis, L. Chasapidis, D. Deloglou, N. Vlachos, A. Kotrba, and G. Anderson, "Investigation of SCR catalysts for marine diesel applications," *SAE Int. J. Engines*, vol. 10, no. 4, pp. 1653–1666, 2017.
- [14] S. Ji, W. Jung, and J. Lee, "Techno-economic evaluation of direct low-pressure selective catalytic reduction for boil-off gas treatment systems of NH₃-fueled ships," *J. Marine Science and Engineering*, vol. 12, no. 5, p. 698, 2024.
- [15] M. I. Foteinos, S. K. Konstantinidis, N. P. Kyrtatos, and K. V. Busk, "Simulation of the transient thermal response of a high pressure selective catalytic reduction aftertreatment system for a Tier III two-stroke marine diesel engine," *J. Eng. for Gas Turbines and Power*, vol. 141, no. 7, p. 071001, 2019.

Date of Received:
September 5, 2025

Date of Accepted:
September 25, 2024

Date of Published:
September 30, 2025
DOI: doi.org/10.30649/ijmea.v2i2.388

PREHEATING TEMPERATURE EFFECT ON FLUX-CORED ARC WELDING (FCAW) IN 3G POSITION ON STEEL PLATE TOWARDS TENSILE STRENGTH AND HARDNESS

Shihab Maulana Imam Saputra¹, Dwisetiono^{2*}, Urip Prayogi², Arif Winarno², Maxima Ari Saktiono²

¹ PT. PAL Indonesia, Surabaya, 60155, Indonesia

² Engineer Profession Education, Widya Mandala Surabaya Catholic University, Indonesia

*Corresponding Author: ddwisetiono@gmail.com

ABSTRACT

Every process, whether planning, testing, or production, must meet established standards and be conducted professionally. Professionalism means that processes are carried out correctly, from procedures and implementation to analysis and decision-making or conclusions. This prevents undesirable outcomes and ultimately ensures the sustainability of the company or its operations. This research was conducted to fulfill the professionalism standards in studying the effect of preheating temperature on welding results, especially on the mechanical properties of the weld, in this case, the tensile strength and hardness of LR Grade (AH36) steel plate welds. This research used the Flux-Cored Arc Welding (FCAW) process with variations in preheating temperature: without preheating, 100°C, and 200°C. The tensile test results showed that the specimen without preheating had the highest tensile strength of 530.28 MPa. Among the preheated specimens, the specimen with preheating at 200°C had the highest average tensile strength of 518.79 MPa. Therefore, it can be concluded that increasing the preheating temperature of the material decreases its tensile strength. Hardness observations showed that higher preheating temperatures caused a decrease in the hardness of the base metal and the Heat-Affected Zone (HAZ), while the hardness of the weld metal increased. Based on these two parameters, it can be concluded that preheating is not optimal for flux-cored arc welding (FCAW) with LR Grade (AH36) material.

Keywords: Flux-cored arc welding, LR grade, preheating, professionalism, ship plate, sustainability

Introduction

Every process, from planning, testing to production, must meet established standards and be executed professionally. Professionalism means that processes are executed correctly, from procedures and implementation to analysis and decision-making or conclusions. This prevents undesirable outcomes and ultimately ensures the sustainability of the company and its operations. This also applies to the shipping industry. In the shipping industry, one of the most frequently performed processes is welding, particularly in the

steel ship industry. The welding method widely used to meet this need is Flux-Cored Arc Welding (FCAW). FCAW is known as a welding process that offers high speed, deep penetration, and can be applied to various welding positions and metal types. This process also allows welding to be performed in open environments, as some types of FCAW wire can provide internal shielding gas (self-shielded) [1][2].

One important factor in the welding process is the preheating temperature. Preheating is the process of heating the material before welding, intending to reduce the temperature difference

between the weld area and the surrounding area [3]. This helps to prevent cracking due to rapid cooling and reduces residual stress that can affect the mechanical strength of the weld joint [4].

In carbon steel welding, especially for steels with medium to high carbon content, preheating is highly recommended as it can prevent the formation of hard and brittle martensite in the heat-affected zone (HAZ). If the preheating temperature is not properly considered, hydrogen cracking may occur, leading to structural failure of the welded joint [5]. Therefore, this study focuses on analyzing the effect of preheating temperature on the tensile strength and hardness of carbon steel weld joints using the FCAW method.

Several previous studies have shown that preheating affects the mechanical properties of weld joints. Increasing the preheating temperature can reduce the cooling rate after welding, resulting in a finer microstructure and toughness of the weld joint [6]. Furthermore, a study found that excessively high preheating temperatures can lead to excessive grain growth, potentially reducing the tensile strength of the weld joint [7]. Therefore, it is important to determine the optimal preheating temperature to achieve the best mechanical properties.

Since ship hull structures must be able to withstand dynamic loads, seawater corrosion, and pressure from waves and cargo, uncontrolled mechanical properties such as tensile strength and toughness in weld joints can lead to cracking or even structural failure during ship operation. Thus, preheating serves as a crucial preventive measure to ensure the integrity of weld joints in ship hull construction.

In the industry, the selection of preheating temperature often refers to established standards such as the AWS D1.1 Structural Welding Code, which recommends a temperature range based on the type of material and plate thickness. However, in practice, the preheating temperature is also influenced by other factors such as the type of electrode used, the cooling method, and environmental conditions during the welding process [8][9].

This study aims to evaluate the effect of varying preheating temperatures on the mechanical properties of carbon steel weld joints, particularly in terms of tensile strength and hardness. The temperature variations used in this study are no preheating, 100°C, and 200°C. Tensile testing is conducted to determine the extent to which the

mechanical strength of the weld joint can withstand tensile forces, while hardness testing is performed to evaluate changes in mechanical properties in the weld and HAZ areas. The results of this study are expected to contribute to the field of welding, particularly in determining optimal preheating parameters to improve the quality of carbon steel weld joints. Additionally, this research may serve as a reference for the manufacturing and construction industries in implementing more effective and efficient welding techniques.

Methodology

a. Research Detail

The steps of the research are to analyze the effect of variations in preheating temperature on the tensile strength of carbon steel welded joints using the FCAW method. Moreover, it analyzes the effect of preheating temperature variations on hardness in the weld area and HAZ. Then, determining the optimal use of preheating or not to obtain the best combination of tensile strength and hardness in carbon steel welded joints.

b. Data Identification

Previous research on the welding process of carbon steel plates of the LR GRADE AH36 type, selecting the appropriate welding parameters is crucial to ensure the quality and strength of the weld joints, particularly in terms of tensile strength and hardness. One critical parameter that must be considered is the preheating temperature, or the initial heating of the material before welding. Preheating is known to affect the cooling rate and heat distribution in the weld area and its surroundings, which directly influences the mechanical properties of the weld.

However, the effect of varying preheating temperatures on the tensile strength of LR GRADE AH36 plates welded using the FCAW method has not been fully understood. Further research is needed to comprehend how changes in preheating temperature—such as no preheating, 100°C, and 200°C—affect the weld joint's resistance to tensile forces.

c. Data Collection

Data collection in this study was carried out experimentally in a laboratory to evaluate the effect of varying preheating temperatures on the tensile strength and hardness of welds produced using the

FCAW method on LR GRADE AH36 carbon steel plates with a 3G (vertical up) welding position. The initial step involved material preparation, including cutting the steel plates into standardized test specimens, followed by surface cleaning to remove contaminants such as oil, rust, or dust that could affect weld quality. The specimens were then grouped based on preheating temperature variations: no preheating (as the control), preheating at 100°C, and preheating at 200°C. Preheating was applied evenly to the welding area using a heating device until the desired temperature was reached, with temperature control monitored using thermocouples and infrared thermometers to ensure consistency [10].

The welding process was conducted using the FCAW method, with welding parameters such as current, voltage, welding speed, and filler wire type kept constant for all specimens to ensure that preheating temperature was the only independent variable. After welding and sufficient cooling, the specimens were cut to prepare samples for tensile and hardness testing [11].

Tensile testing was performed using a Universal Testing Machine (UTM) in accordance with the AWS D1.1 standard, where each specimen was pulled until fracture to obtain the maximum tensile strength value (Ultimate Tensile Strength/UTS). Meanwhile, hardness testing was conducted using the Vickers Hardness Test method, also based on AWS D1.1 standards. Hardness was measured at three key locations: the weld metal (WM), the heat-affected zone (HAZ), and the base metal (BM), to observe how different preheating temperatures affected the hardness distribution across the weld area.

All data obtained from the testing were carefully recorded, both manually and using supporting software. Additionally, every step of the testing process was documented with photographs and technical notes to ensure traceability of data. The collected data were then analyzed quantitatively to identify trends and changes, and to compare the results across the different preheating temperature conditions, ultimately concluding their effects on the mechanical properties of the welded joints.

d. Data Analysis

The data analysis will be conducted based on the results of tensile strength and hardness tests from each specimen welded with different preheating temperatures, namely without preheating, at

100°C, and at 200°C. The purpose of this analysis is to evaluate the extent to which preheating temperature influences the mechanical properties of welded joints on LR GRADE AH36 carbon steel plates welded using the Flux-Cored Arc Welding (FCAW) method in the 3G (vertical up) position [4][5].

e. The Effect of Preheating Temperature on the Tensile Strength of Welded Joints

Preheating temperature in the welding process plays an important role in determining the quality of the weld joint, particularly its tensile strength. Tensile strength is one of the main mechanical parameters used to assess a material's resistance to tensile forces until fracture occurs. In welded joints, tensile strength is influenced by the microstructure formed during the process, which is significantly affected by thermal parameters such as preheating temperature.

f. Tensile Test

Each material has different properties (flexibility, hardness, toughness, etc.). To determine the mechanical properties of a material, testing is required—tensile testing is one of the most commonly performed tests. This test is used to determine the strength level of a material and to identify its characteristics [12].

A tensile testing machine operates by pulling the specimen axially, from both ends, until the specimen undergoes plastic deformation and eventually breaks. During the pulling process, a change in length occurs at the center of the specimen, and a measuring device accurately records this elongation relative to the applied load. From this data, several key parameters are calculated, such as the UTS, yield strength, modulus of elasticity (Young's modulus), and total elongation.

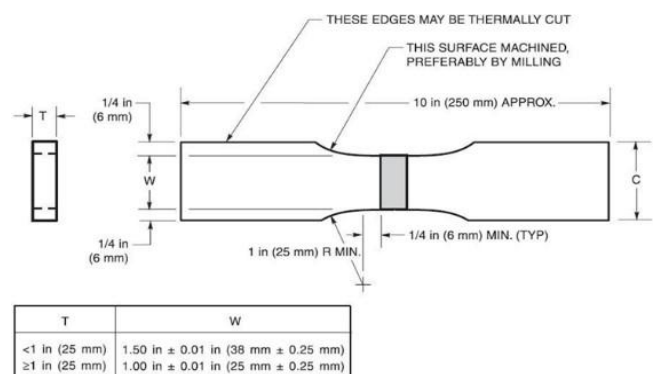


Figure 1. Examples of Tensile Test

g. Hardness Test

The hardness test aims to determine a material's resistance to plastic deformation caused by external loads. A commonly used method for testing the hardness of shipbuilding steel is the Vickers hardness test (HV), which is suitable for materials with small thicknesses and smoother surfaces.

The Vickers method involves pressing a diamond indenter, shaped like a pyramid with a square base and an angle of 136 degrees between opposite faces, into the surface of the test material or specimen. This indentation process creates a mark or impression on the material's surface. The hardness value is determined by measuring the average diagonal length of the indentation using a microscope.

One of the main reasons for conducting a hardness test on welded joints is to avoid the potential formation of martensitic structures, especially in medium- to high-carbon steels. Martensite is a very hard but brittle structure, prone to cracking, particularly under cold conditions or when hydrogen is absorbed into the weld metal. If the measured hardness value in the HAZ exceeds the standard limit (e.g., above 350 HV for carbon steels), the joint is considered at high risk of hydrogen-induced cracking (HIC) and typically must be repaired or subjected to Post-Weld Heat Treatment (PWHT) to reduce its hardness.

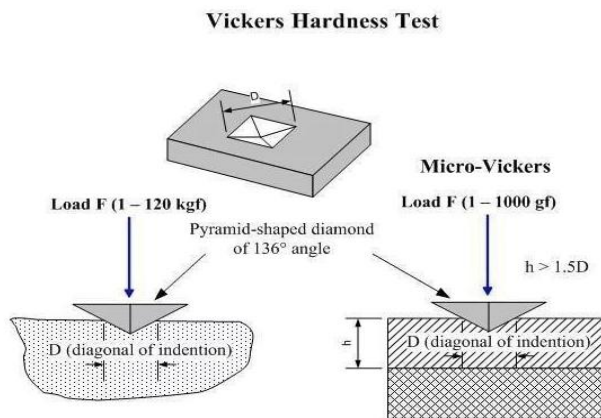


Figure 2. Examples of Hardness Test

Result and Discussion

a. Welding Procedure Specification (WPS)

The welding process was carried out at PT PAL INDONESIA. The testing of the welded specimens was conducted at the Material Testing Laboratory of PT PAL INDONESIA. Welding was performed on

LR GRADE (AH36) steel plates with the following specifications: length 300 mm, width 300 mm (2 plates), and thickness 11 mm. A bevel was made on one side of the plate before welding. The welding process followed the parameters specified in the WPS applicable at PT PAL INDONESIA.

The WPS is a qualified written document prepared as a guideline for welding operators during the welding process to ensure compliance with all required standards and codes. WPS is a mandatory standard that must be met and is a prerequisite in the welding process used in the operation of industrial tools or machines that involve welding. The WPS must be prepared before performing any welding operations. It is also implemented in the welding of various industrial equipment or machinery, such as heat exchangers, pressure vessels, and other equipment that involves welding applications.

b. WPS on Plates without Preheating.

Based on the WPS that was prepared before the welding process, the LR GRADE (AH36) plate material without preheating consists of three welding layers, with a ceramic backing applied beforehand. The ceramic backing functions as a support to improve weld penetration and to produce a neater and stronger weld. Each welding layer is described as follows:

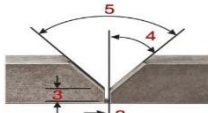
The first layer is the root weld, which serves as the base welding on the material. In this stage, the electrode used is AWS A5.20 type with a diameter of 1.2 millimeters. The current applied during the root weld is 17 Amperes, and the voltage is 26.8 Volts. From the recorded time for one root weld pass, it took 3.45 minutes, resulting in a welding travel speed of 87 mm/min. The polarity type used DCEM.

The second layer is the filling weld, which serves to fill the joint in the material. In this stage, the electrode used is AWS A5.20 type with a diameter of 1.2 millimeters. The current used during the weld is 17 Amperes, and the voltage is 26.8 Volts. Based on the recorded time for one pass of the filling weld, it took 1.26 minutes, resulting in a welding travel speed of 238 mm/min. The polarity type used is DCEM.

The third layer is the weld cap area. In this stage, the electrode used is AWS A5.20 type with a diameter of 1.2 millimeters. The current used during the weld is 17 Amperes, and the voltage is 26.8 Volts. Based on the recorded time for one pass

Table 1. WPS without preheating

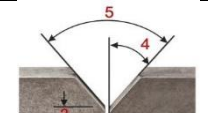
WELDING PROCEDURE							
Weld Layer (s)	Process	Filler Metal		Current		Volt Range (V)	Travel Speed Range (mm/min)
		Class	Diameter (mm)	Type of Polarity	Amp. Range (A)		
1st	FCAW	AWS A5.20	1,2	DCEM	15-19	25-28	60 – 90
2nd	FCAW	AWS A5.20	1,2	DCEM	15-19	25-28	80 – 140
3rd	FCAW	AWS A5.20	1,2	DCEM	15-19	25-28	80 – 140



Joint Detail

Table 2. WPS preheating 100°C


WELDING PROCEDURE							
Weld Layer (s)	Process	Filler Metal		Current		Volt Range (V)	Travel Speed Range (mm/min)
		Class	Diameter (mm)	Type of Polarity	Amp. Range (A)		
1st	FCAW	AWS A5.20	1,2	DCEM	15-19	25-28	60 - 90
2nd	FCAW	AWS A5.20	1,2	DCEM	15-19	25-28	80 - 140
3rd	FCAW	AWS A5.20	1,2	DCEM	15-19	25-28	80 - 140



Joint Detail

Table 3. WPS preheating 200°C

WELDING PROCEDURE							
Weld Layer (s)	Process	Filler Metal		Current		Volt Range (V)	Travel Speed Range (mm/min)
		Class	Diameter (mm)	Type of Polarity	Amp. Range (A)		
1st	FCAW	AWS A5.20	1,2	DCEM	15-19	25-28	60 - 90
2nd	FCAW	AWS A5.20	1,2	DCEM	15-19	25-28	80 - 140
3rd	FCAW	AWS A5.20	1,2	DCEM	15-19	25-28	80 - 140



Joint Detail

of the cap weld, it took 2.6 minutes, resulting in a welding travel speed of 115.3 mm/min. The polarity type used is DCEM.

c. WPS for Plate Welding with Preheating at 100°C

Based on the Welding Procedure Specification (WPS) data prepared before the welding process,

the LR GRADE (AH36) plate material undergoes a preheating process consisting of three welding layers. Each welding layer is explained as follows.

The first layer is the root weld on the material. In this stage, the electrode used is AWS A5.20 type with a diameter of 1.2 millimeters. The current used for the root weld is 17 Amperes, and the voltage is 26.8 Volts. Based on the recorded time for one pass

of the root weld, it took 4.02 minutes, resulting in a welding travel speed of 74.6 mm/min. The type of polarity used (DCEN).

The second layer is the filling weld on the material. In this stage, the electrode used is also AWS A5.20 type with a diameter of 1.2 millimeters. The current used remains 17 Amperes, and the voltage is 26.8 Volts. The recorded time for one pass of the filling weld is 2 minutes, resulting in a welding travel speed of 150 mm/min. The type of polarity used (DCEN).

The third layer is the weld cap area. In this stage, the electrode used is the AWS A5.20 type with a diameter of 1.2 millimeters. The current used for the cap weld is 17 Amperes, and the voltage is 26.8 Volts. The recorded time for one pass of the cap weld is 2.43 minutes, resulting in a welding travel speed of 123 mm/min. The type of polarity used is DCEN.

d. WPS for Plate Welding with Preheating at 200°C

Based on the WPS data prepared before the welding process, the LR GRADE (A536) plate material undergoes a preheating process consisting of three welding layers. Each welding layer is explained as follows.

The first layer is the base welding on the material (root weld). In this stage, the electrode used is of AWS A5.20 type with a diameter of 1.2 millimeters. The current used in the root weld is 17 Amperes, and the voltage is 26.8 Volts. From the recorded time for one pass of the root weld, it took 4.02 minutes, resulting in a welding travel speed of 74.6 mm/min. The polarity type used is DCEN.

The second layer is the filling weld on the material. In this stage, the electrode used is also of AWS A5.20 type with a diameter of 1.2 millimeters. The current used is 17 Amperes, and the voltage is 26.8 Volts. The recorded time for one pass of the filling weld is 2 minutes, resulting in a welding travel speed of 150 mm/min. The polarity type used is DCEN.

The third layer is the weld cap area (cap). In this stage, the electrode used is of AWS A5.20 type with a diameter of 1.2 millimeters. The current used in the cap weld is 17 Amperes, and the voltage is 26.8 Volts. The recorded time for one pass of the cap weld is 2.43 minutes, resulting in a welding travel speed of 123 mm/min. The polarity type used is DCEN.

e. Visual Test

Visual inspection was carried out as an initial stage in the series of tests to assess the quality of the weld joint. This test aims to identify the presence of surface defects directly without damaging the specimen. In this study, the visual inspection was conducted after the welding process was completed and the weld metal had fully cooled. The examination was performed using bright lighting, a magnifying glass, and a weld gauge to evaluate the geometric dimensions of the weld cross-section.

The visual observation results on all specimens indicated no significant surface defects. The surface of the weld metal appeared smooth and uniform, with a consistent and neat weld bead appearance, and showed good fusion between the weld metal and the base metal. No cracks, open porosity (blow holes), undercut, overlap, slag inclusion, or excessive spatter were found on the weld surface.

Overall, the visual inspection results support the success of the welding parameters designed in this procedure and provide a strong basis to proceed to the next stage of destructive testing. The absence of visual defects also strengthens the assumption that the weld joint has good structural integrity, is fit for use, and meets the visual standard criteria based on AWS D1.1 and ISO 5817 level B (stringent).

f. Test Visual Objectives

Visual testing (VT) is the most basic non-destructive testing (NDT) method used to evaluate the surface condition of welded joints. Its purpose is to ensure that the weld is free from any visible defects and meets established quality standards before further testing is conducted.

g. Observation result

After a thorough inspection of all test specimens at varying preheating temperatures, no visual defects were found. The following are the general findings of the visual inspection:

1. Uniform weld path, no deviations in direction or shape.
2. Smooth weld surface and free of slag, spatter, or contamination.
3. No open porosity.
4. No undercuts or overlaps.
5. No microcracks at the root or weld surface.
6. No arc strikes observed outside the weld zone.



Figure 2. Welding results without preheating



Figure 3. Welding results initial heating 100°C



Figure 4. Welding results initial heating 200°C

h. Mechanical Testing

Mechanical testing is a series of tests conducted on materials to determine their mechanical properties, such as strength, hardness, toughness, and ductility. The main objective of this testing is to ensure that the material (including weld joints) can withstand loads and forces during service without failure. The superior properties of a material can be

matched to its intended application. There is a tendency for some mechanical properties to be inversely related, meaning that optimizing certain properties often comes at the expense of others. Therefore, selecting a suitable material and applying the right treatment becomes essential to optimize these properties according to the specific requirements.

Mechanical testing is a critical part of weld quality assessment because it provides a quantitative understanding of the material's strength and resistance to applied loads. In the context of welding, mechanical tests are used to evaluate whether the weld results meet technical specifications and quality standards, particularly in terms of tensile strength and hardness of the joint. These tests not only measure the joint's resistance to external forces but also reflect the microstructural condition and the success of fusion between metals. In this study, two main types of mechanical tests were carried out: tensile testing and hardness testing, both of which aim to evaluate the welding results using the FCAW method on steel plates in the 3G position.

i. Tensile Strength Test

Tensile testing is carried out to determine the extent to which a welded joint can withstand axial tensile forces before failure or fracture occurs. This test serves as a primary indicator of the success of the welding process, as it reveals the strength of fusion between the weld metal and the base metal, as well as the microstructural condition along the weld zone. In this study, tensile tests were performed on specimens welded using the FCAW method in the 3G position on steel plates, both with and without the application of preheating.

The experimental device used for tensile testing must have strong grips and high stiffness. The tensile test is conducted in accordance with a specific standard. In this final project, the tensile testing refers to the AWS D1.1 standard. The test specimens were prepared based on AWS D1.1-09 specifications, with dimensions of 300 mm in length, 38 mm in width, and 11 mm in thickness, with a minimum radius of 60 mm.

The results of the tensile test are presented in the form of a graph. The graph shows the yield stress and maximum stress of the material being tested. The graph also identifies the fracture zones that occurred during the specimen testing. The

Table 4. Non-preheating tensile test calculation results

Test Piece Code	Visual	A0 (WxT) mm ²	p.yield (kgf)	P.max (kgf)	Yield Strength (MPa)	Tensile Strength (MPa)	L0 (mm)	L1 (mm)	E (%)	Breaking
Non	Good	(25,3x11) 278,3	11.000	15.050	387,55	530,28	50	67	34	Base metal

Table 5. Calculation results of tensile preheat 100°C

Test Piece Code	Visual	A0 (WxT) mm ²	p.yield (kgf)	P.max (kgf)	Yield Strength (MPa)	Tensile Strength (MPa)	L0 (mm)	L1 (mm)	E (%)	Breaking
100	good	(25x11) 275	10.850	14.550	386,86	518,79	50	64	28	Weld Metal

Table 6. Calculation results of tensile preheat 200°C

Test Piece Code	Visual	A0 (WxT) mm ²	p.yield (kgf)	P.max (kgf)	Yield Strength (MPa)	Tensile Strength (MPa)	L0 (mm)	L1 (mm)	E (%)	Breaking
100	good	(25,4x11) 279,4	10.450	14.525	366,75	509,76	50	68	36	Base metal

following describes the results of each test and the tensile test calculations for each specimen.

Table 7. Minimum results of tensile test calculation

Mechanic Properties	Minimum Value LR AH36
Yield Strength (YS)	≥ 355 MPa
Tensile Strength (UTS)	490 Mpa
Elongation ($L_0 = 5.65\sqrt{A}$)	≥ 21%

From the tensile test data based on calculations in Tables 4.4 to 4.6, it is found that preheating treatment affects the tensile strength of LR Grade (AH36) steel. The results of this thesis research showed that specimens given 200°C preheating treatment had the lowest tensile strength of 509.76 MPa, and one of the test materials experienced fracture in the base metal. specimens with 100°C preheating had a tensile strength value of 518.79 MPa. specimens without preheating had the highest average tensile strength of 530.041 MPa.

From the specimen without preheating to the one treated with a preheating temperature of 200°C, the tensile strength decreased progressively. This decline in tensile strength was directly proportional to the increasing preheating temperature. The reduction is attributed to the

influence of higher preheating temperatures, which lead to less effective penetration during the welding process, thereby resulting in poor fusion between the base metal and weld metal.

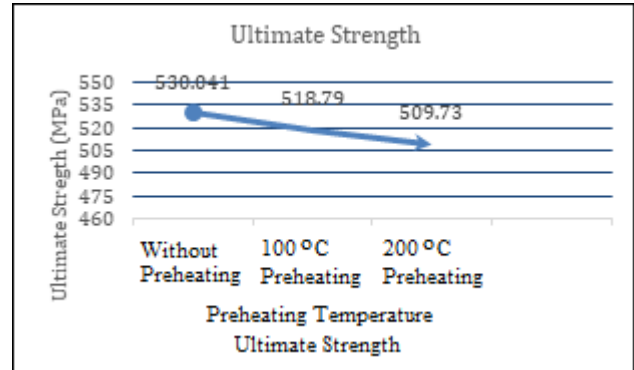


Figure 5. Ultimate Strength Specimen Graph

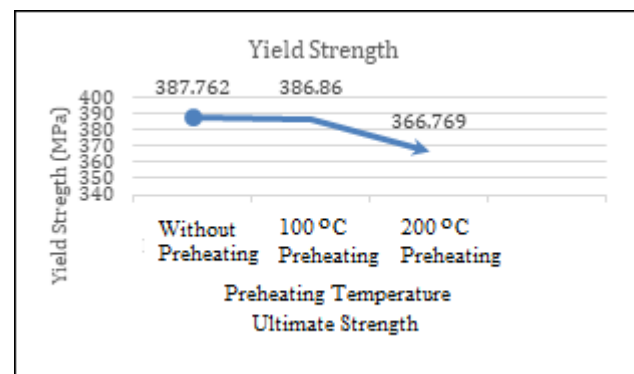


Figure 6. Yield Strength Specimen Graph

Table 8. Hardness test results data of specimens without preheating

Location	Vickers Hardness								
	Weld metal			HAZ			Base Metal		
	1	2	3	1	2	3	1	2	3
200° C	201,21	203,32	205,47	182,64	183,82	186,64	184,61	179,92	182,64
Average	203,33			184,36			182,40		

Table 9. Hardness test results data of specimens preheated to 100°C

Location	Vickers Hardness								
	Weld metal			HAZ			Base Metal		
	1	2	3	1	2	3	1	2	3
100° C	201,21	200,57	204,42	185,44	200,89	187,56	187,24	184,61	189,14
Average	202,06			191,29			187,87		

Table 10. Hardness test results data of specimens preheated to 200°C

Location	Vickers Hardness								
	Weld metal			HAZ			Base Metal		
	1	2	3	1	2	3	1	2	3
Without preheat	179,92	182,32	181,51	181,78	201,89	193,08	187,28	198,79	198,25
Average	181,25			192,25			194,77		

j. Vickers Hardness Test

In this study, the hardness test was performed using the Vickers Microhardness method, which was chosen due to its accuracy in measuring narrow regions and its ability to detect even small variations in hardness. The testing instrument used was a microhardness tester with a load of 1 kilogram (HV1) and a dwell time of 10–15 seconds. The test was carried out on FCAW weld specimens in the 3G position, both with and without preheating treatment.

Before testing, the specimens were cross-sectioned perpendicular to the welding direction and polished until the surface was smooth and even.

The data in Table 8 shows the results of specimen hardness tests without preheating temperature in the base metal, HAZ, and weld metal areas. Each area was sampled at three pressure points so that each specimen was tested nine times. From the test results above, the average nominal value for the weld metal was 181.25 VHN, HAZ 192.25 VHN, and base metal 194.77 VHN. The lowest hardness value was due to rapid cooling,

which resulted in a softer weld metal. Meanwhile, in the HAZ and Base Metal areas, the hardness was high because the HAZ area

experienced very rapid cooling (quenching). This rapid cooling can cause martensite transformation in carbon or alloy steel, resulting in a hard but brittle structure.

The data in Table 9 is the result of the hardness test of specimens that were given a preheating temperature treatment of 100°C in the areas of base metal, HAZ, and weld metal. Each area was sampled at three points, so each specimen underwent nine indentation tests.

From the test results above, the average nominal values were obtained as follows: weld metal 202.06 VHN, HAZ 191.29 VHN, and base metal 187.87 VHN. In the weld metal area, the value increased due to the slower cooling, which prevented the formation of soft structures. Meanwhile, in the HAZ and base metal areas, the value decreased due to the increase in the initial temperature of the metal before the welding process. As a result, after welding, the metal did not cool directly from high temperature to room temperature, and the cooling occurred more slowly. This prevented the formation of martensite (a hard structure). Instead, ferrite and pearlite, which are softer, were formed.

The data in Table 10 is the result of the hardness test of welded specimens without preheating temperature treatment, in the areas of weld metal, HAZ, and base metal. Each area was sampled at

three points, so each specimen underwent nine indentation tests.

From the test results above, the average nominal values were obtained as follows: weld metal 203.33 VHN, HAZ 184.36 VHN, and base metal 182.40 VHN. In this treatment, the base metal and HAZ areas had the lowest hardness values, while the weld metal had the highest hardness value. This was caused by the tempering effect on the base metal and the slow cooling that caused the HAZ to form a soft structure.

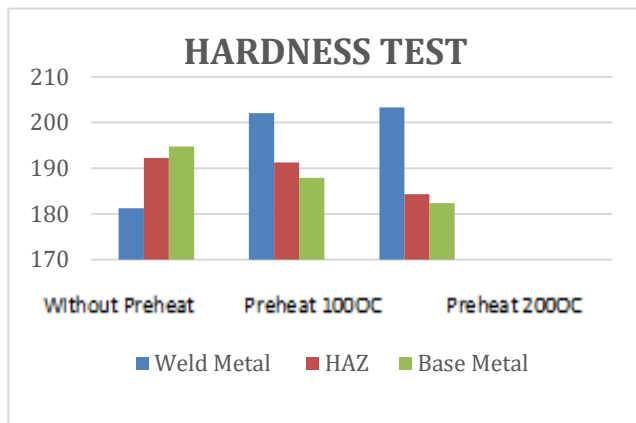


Figure 7. Hardness test results

From the graph above, it can be concluded that preheating treatment affects the mechanical properties of the material, especially the hardness properties. The material experiences an increase in hardness value in the weld metal due to the influence of the heat received by the specimen during the preheating process, which causes the higher temperature, the harder the specimen is treated. Meanwhile, in the base metal and HAZ areas, the higher the preheating temperature given, the lower the hardness value of the metal. This is because at low preheat or without preheat, rapid cooling can form a very hard but brittle martensite or bainite structure. High preheats, the HAZ zone experiences the formation of large and soft grains, resulting in a decreased hardness value. Then, in the base metal zone, the greater the preheat, some of the heat spreads to the base metal, causing a mild "tempering" effect near the HAZ. This effect makes the base metal softer and less tense.

Conclusion

From the results of the previous discussion, the following conclusions can be drawn:

1. The result of the mechanical test, specifically the tensile strength, showed that the specimen

without preheating had the highest average tensile strength value of 530.28 MPa, while the specimen with preheating at a temperature of 200°C had the lowest average tensile strength value of 518.79 MPa. Therefore, it can be concluded that the higher the preheating temperature applied to the material, the lower its tensile strength becomes.

2. The hardness test results showed that the specimen with the highest hardness values in the base metal and Heat Affected Zone (HAZ) areas was the one without preheating. Conversely, the specimen with the lowest hardness in the weld metal area was also the one that did not undergo preheating. Thus, it can be concluded that preheating treatment affects the hardness values in the welded area, where preheating tends to reduce hardness in the base metal and HAZ areas, but can increase hardness in the weld metal area.
3. From the series of tests carried out and the data processing conducted, it can be determined that the application of preheating temperature is less optimal for FCAW (Flux-Cored Arc Welding) on LR Grade (AH36) ship steel plate.

References

- [1] M. Z. Afkari, S. R. I. Hastuty, M. A. Barrinaya, M. U. H. A. M. M. A. D. Awwaluddin, M. S. Anwar, G. K. Sunnardianto, and F. A. I. S. A. L. Mahmuddin, "Analysis of voltage, current density, and welding speed of flux core arc welding on the hardness and micro-structure of high strength low alloy (ASTM A572)," *Key Engineering Materials*, vol. 948, pp. 33–39, 2023.
- [2] C. Kjeldgaard, *FCAW Equipment and Setup, Welding Theory Fundamentals*, 2025.
- [3] J. Yuan, H. Ji, Y. Zhong, G. Cui, L. Xu, and X. Wang, "Effects of different pre-heating welding methods on the temperature field, residual stress and deformation of a Q345C steel butt-welded joint," *Materials*, vol. 16, no. 13, p. 4782, 2023.
- [4] J. C. Lippold and D. J. Kotecki, *Welding Metallurgy and Weldability of Stainless Steels*, Hoboken, NJ, USA: John Wiley & Sons, 2005.
- [5] J. J. Perdomo and L. A. Ganhao, "Failures related to welding," in *Analysis and Prevention of Component and Equipment Failures*, ASM International, 2021, pp. 266–306.
- [6] Y. Wang, H. Zhang, and X. Liu, "Effect of preheating temperature on the mechanical properties of welded joints in high-strength steels," *Journal of Materials Processing Technology*, vol. 255, pp. 178–185, 2018.

- [7] S. Kou, *Welding Metallurgy*, Hoboken, NJ, USA: John Wiley & Sons, 2003.
- [8] American Welding Society (AWS), *AWS D1.1 Structural Welding Code – Steel*, Miami, FL, USA: AWS, 2015.
- [9] P. Majumder, A. Sinha, and A. Biswas, "Effect of preheating techniques on bead geometry and microhardness of weldment developed through the submerged arc welding process," *Materials Today: Proceedings*, vol. 46, pp. 5001–5007, 2021.
- [10] D. Dwisetiono and R. Dikrulloh, "The effect of welding position and filler diameter on the results of welding propeller leaves with gas metal arc welding," *Zona Laut*, vol. 3, no. 1, pp. 15–23, 2022.
- [11] D. Dwisetiono and A. M. N. C. Kurniawan, "Perbandingan hasil pengelasan GMAW dan FCAW pada welding repair propeller berbahan kuningan," *Journal of Mechanical Engineering, Manufactures, Materials and Energy*, vol. 7, no. 1, pp. 36–42, 2023.
- [12] D. B. Firmansyah, "Analisa kekuatan rangkaudukan cylinder hidrolik," *Jurnal Teknik Mesin Mercur Buana*, vol. 8, no. 3, pp. 18–32, 2020.

Date of Received:
September 17, 2025

Date of Accepted:
September 26, 2025

Date of Published:
September 30, 2025
DOI: doi.org/10.30649/ijmea

THE EFFORTS TO IMPROVE REPAIR AND MAINTENANCE ON THE SHIP ENGINE TO OVERCOME OVER NOISE

Cahya Kusuma^{1*}, Mahendra Indriaryanto²

¹Akademi Angkatan Laut, 60178, Indonesia

²Research Center for Hydrodynamics Technology, National Research and Innovation Agency, 60111, Indonesia

*Corresponding Author: kusumacahya99@gmail.com

ABSTRACT

The noise generated by ship engines is a significant environmental issue in the maritime industry. This research aims to identify noise sources, assess their impact on human health and the environment, and develop effective strategies for improvement and maintenance. Research methods include identifying noise sources through field surveys and noise measurements, followed by data analysis to determine their impacts. Literature reviews on the basic concepts of noise in the maritime environment and previous related studies form the basis of understanding in this research. The results of this study are expected to provide valuable recommendations for reducing the impact of ship engine noise on the environment and human health. This research is expected to make a significant contribution to improving the sustainability of the maritime industry by enhancing environmental quality and worker well-being.

Keywords: Biodiesel, eco-friendly ship, motor performance, numerical investigation

Introduction

Explain the background, novelty, and objectives of the research. Noise pollution from ship engines is a significant concern in marine environments worldwide. The primary sources of noise on ships are the main engines and auxiliary equipment, which generate both sound and vibrations. Tonal and harmonic components can be detected in noise emissions, with frequencies depending on engine characteristics [1]. Marine noise pollution can have adverse effects on marine fauna, altering their behavior, physiology, and ecology. Anthropogenic noise sources, such as maritime traffic, shipping, and high-powered sonar, contribute to the rising levels of ocean noise pollution [2]. The COVID-19 pandemic led to a reduction in maritime traffic, resulting in lower noise levels in marine environments [2]. Governments and marine researchers have established response plans to address the problem of underwater noise pollution

[2]. Moreover, prolonged exposure to high noise levels can cause stress and even physical harm to marine animals. Therefore, finding solutions to reduce noise emissions from ship engines is crucial to safeguarding the health and well-being of marine ecosystems.

One potential solution to this problem is the development and implementation of quieter engine technologies. By investing in research and innovation, engineers can design ship engines that generate less noise without compromising performance. Another approach is to establish and enforce regulations that limit ship noise emissions, similar to those already applied to air and land vehicles. In addition, educating ship operators and crews about the importance of reducing noise pollution and adopting noise mitigation practices can also help minimize the impact of ship engine noise on marine life. By taking these steps, we can work toward a future where marine ecosystems are

no longer threatened by the harmful effects of noise pollution.

This effort will not only benefit marine life but also the communities that depend on healthy oceans for their survival. Implementing these measures may require collaboration between governments, industry leaders, and environmental organizations, but the long-term benefits make it highly worthwhile. By working together to address ship engine noise pollution, we can create a more sustainable and harmonious relationship between humans and the marine environment. This collaboration may include stricter regulations on ship noise emissions, investments in quieter engine technologies, and the establishment of marine protected areas where noise pollution is minimized. By taking these proactive steps, we can help ensure the long-term health and vitality of our oceans for future generations to enjoy. We must prioritize the protection of marine ecosystems and work collectively toward a more sustainable future for our planet.

One of the primary ways to address noise pollution in marine environments is by promoting the use of quieter engine technologies in ships. By investing in research and development of quieter engines, we can significantly reduce the impact of noise pollution on marine life. Additionally, enforcing stricter regulations on ship noise emissions can help limit the harmful effects of sound pollution on underwater ecosystems. Marine protected areas where noise pollution is minimized can also provide safe havens for marine life to thrive without constant human-made disturbances. By working together to combat ocean noise pollution, we can build a more sustainable and harmonious relationship between humans and the marine environment.

In addition to its environmental impacts, addressing ocean noise pollution is also critical for the safety and well-being of marine life. Excessive noise can interfere with the communication, navigation, and feeding patterns of marine animals, leading to increased stress and even physical harm. For example, loud ship noise can disrupt the orientation of marine mammals, causing them to become stranded or collide with vessels. Reducing noise pollution creates a safer and more peaceful environment for marine species to thrive, which is especially important for species that rely on sound for activities such as echolocation. Furthermore, lowering noise levels can help prevent disturbances in breeding and feeding grounds vital to marine

species. By addressing ocean noise pollution, we can help protect the delicate balance of marine ecosystems and ensure the well-being of the diverse species that call the oceans home. Ultimately, creating a quieter marine environment is essential for the safety and comfort of marine life and is crucial for maintaining a healthy and thriving ocean ecosystem.

Several strategies for reducing ocean noise pollution include enforcing stricter regulations on ship and boat engines, adopting quieter technologies for offshore construction projects, and establishing marine protected areas where sound levels are closely monitored and controlled. Additionally, raising awareness about the impacts of noise pollution on marine life and promoting more sustainable practices within the ocean industry can play a significant role in mitigating this environmental threat. Collaboration between governments, industries, and conservation organizations is vital to addressing this issue and working toward a quieter, more harmonious marine environment for all ocean life.

Methodology

a. Identification of Noise Sources

- **Field Survey:** Conduct surveys on ships to identify the main sources of noise.
- **Noise Measurement:** Use noise meters to measure noise levels from various engine components.

b. Impact Analysis

- **Data Analysis:** Analyze measurement data to determine the effects of noise on human health and the environment.
- **Literature Review:** Conduct a literature review to understand the long-term impacts of noise on ship machinery and structures.

c. Development of Improvement and Maintenance Strategies

- **Expert Consultation:** Engage with marine engineers and noise specialists to develop effective improvement strategies.
- **Testing:** Carry out trials of the recommended improvement and maintenance strategies.

d. Evaluation of Results

- **Effectiveness Analysis:** Assess the effectiveness of improvement and maintenance strategies based on repeated

noise measurements and feedback from crew members.

Result and Discussion

A regular maintenance schedule is essential to ensure the smooth functioning of ships. By adhering to this schedule, shipowners and operators can avoid costly repairs and unexpected breakdowns. Proper maintenance also helps extend the lifespan of ship machinery and equipment, ultimately saving money in the long run. Overall, investing in regular maintenance is a critical aspect of ensuring the safety and efficiency of maritime operations. Without routine maintenance, ships are at risk of damage that could lead to serious accidents or operational delays. By investing in proper maintenance, shipowners can also ensure compliance with maritime regulations and standards, reducing the likelihood of legal consequences. Furthermore, well-maintained ships are more appealing to potential charterers and clients, thereby enhancing the reputation and profitability of maritime businesses. Ultimately, prioritizing regular maintenance is not only a matter of safety but also a smart business decision for shipowners and operators.

Routine maintenance of ship engines is vital to ensure longevity and efficiency. An appropriate schedule should be established to guarantee that all inspections and necessary replacements are carried out on time. This not only prolongs the lifespan of ship engines but also contributes to the overall safety of the vessel and its crew. By adhering to strict maintenance routines, ship operators can minimize the likelihood of unexpected breakdowns or failures at sea. Additionally, investing in high-quality spare parts and skilled technicians can enhance the reliability and performance of ship engines, ultimately leading to smoother and more efficient maritime operations.

Experienced technicians are crucial for maintaining the efficiency and reliability of ship machinery. Using substandard or low-quality parts increases the risk of equipment failure and potential safety hazards. Therefore, ship operators must prioritize the use of high-quality engine components to ensure optimal performance and longevity. Regular inspections and maintenance by trained professionals can help identify potential issues before they escalate into major problems. Overall, investing in premium engine parts and skilled technicians is essential for smooth

operations and ship safety. This approach not only guarantees the safety of crew and passengers onboard but also reduces the risk of costly repairs and operational disruptions. By staying proactive and vigilant in maintenance practices, ship operators can extend engine lifespan and avoid unexpected failures at sea. Ultimately, prioritizing high-quality components and expert services is a smart long-term investment, crucial for the success and efficiency of maritime operations.



Figure 1. Maintenance on ships experiencing noise issues

Maintenance in engine rooms and other key areas can also significantly improve crew comfort and well-being, while reducing noise pollution for nearby marine life. Additionally, regular inspection and upkeep of soundproofing materials are necessary to ensure they remain effective and in good condition. Proper ventilation and cooling systems must also be installed to prevent overheating and maintain optimal engine performance. All these factors contribute to safe and efficient maritime operations, underscoring the importance of attention to detail and quality in every aspect of ship maintenance and operation. This not only improves overall crew welfare but also enhances their productivity and performance onboard. Moreover, proper ventilation and cooling systems play a crucial role in preventing engine overheating, ultimately leading to better fuel efficiency and lower emissions. In summary, meticulous attention to detail in ship maintenance and operations is vital for successful and sustainable maritime activities.

The implementation of vibration-damping and soundproofing materials in cargo ship engine rooms resulted in a significant reduction in noise levels, improving working conditions for crew members and lowering the risk of hearing damage. The success of this project highlights the positive impact of investing in high-quality noise reduction measures.

The retrofitting of passenger ferries with advanced mufflers and exhaust systems led to a marked decrease in noise pollution, enhancing the overall passenger experience while meeting strict environmental regulations. This case study demonstrates the effectiveness of proactive noise reduction strategies in the maritime industry, emphasizing the importance of prioritizing crew and passenger well-being.

Improvements to waste disposal systems and the implementation of soundproofing materials on cruise ships have resulted in a significant reduction in noise levels, creating a more pleasant and peaceful environment for guests. This investment not only enhances customer satisfaction but also contributes to the company's overall sustainability goals. By taking proactive steps to address noise pollution, maritime companies can improve their reputation, attract more clients, and demonstrate their commitment to environmental responsibility.

In conclusion, prioritizing noise reduction measures in the maritime industry not only benefits the health and well-being of individuals onboard but also has long-term positive effects on the environment and the overall success of maritime businesses.



Figure 2. Briefing by the project manager regarding engine maintenance

Training crew members in noise reduction techniques can also improve efficiency and productivity onboard. By educating the crew about the importance of minimizing noise levels, companies can foster a culture of environmental awareness and responsibility. This can lead to reduced fuel consumption, lower maintenance costs, and a more harmonious working environment for all staff. Furthermore, training crew members in noise reduction practices can help prevent hearing loss and other health issues associated with long-term exposure to high noise levels. Overall, investing in crew education and

training in this area can provide broad benefits for both individuals and companies.

Conclusion

Considering the importance of addressing noise in ship engines and the potential benefits of investing in crew training on noise reduction techniques, companies can achieve more than just operational improvements. By prioritizing environmental responsibility along with employee health and safety, companies can not only enhance their outcomes through cost reduction and improved efficiency but also contribute to a more sustainable future for the maritime industry as a whole.

In conclusion, addressing ship engine noise is not merely a matter of regulatory compliance but a strategic decision that can have long-term positive impacts on both business performance and the environment.

The key strategies for reducing noise pollution in maritime operations include investing in crew training on noise reduction techniques, prioritizing environmental responsibility and employee health and safety, and contributing to the industry's long-term sustainability. By taking these steps, companies can not only improve their bottom line but also make a positive impact on the environment and the overall sustainability of the maritime sector. Clearly, addressing ship engine noise is a strategic decision that offers long-term benefits for both businesses and the environment.

Acknowledgments

We thank the UHT marine engineering study program for launching its first journal IJMEA, hopefully it will be useful. thank you also for the publication of the results of this research. congratulations.

References

- [1] Nadia and Hanan, "Recent progress in marine noise pollution: A thorough review," *Chemosphere*, 2022.
- [2] Claire Renée and Stephanie, "A global review of vessel collisions with marine animals," *Frontiers in Marine Science*, 2020.
- [3] Sarah, Renée, Joshua, Leah, and Clare, "The effects of ship noise on marine mammals: A review," *Frontiers in Marine Science*, 2019.
- [4] Tomaso, Enrico, and Corrado, "Noise mapping," *Noise Mapping Journal*, 2016.

- [5] L. A. van Gunsteren and C. Pronk, *Propeller Design Concepts*, Technical Papers, LIPS BV, Drunen, Holland.
- [6] G. Kuiper, *The Wageningen Propeller Series*, MARIN, 1992.
- [7] ISO 10534-2, *Acoustics — Determination of Sound Absorption Coefficient and Impedance in Impedance Tubes — Part 2: Transfer-Function Method*, 1998.
- [8] ASTM E1050-19, *Standard Test Method for Impedance and Absorption of Acoustical Materials Using a Tube, Two Microphones, and a Digital Frequency Analysis System*, 2019.
- [9] H. Medwin and C. S. Clay, *Fundamentals of Acoustical Oceanography*, in *Fisheries Oceanography*, vol. 8, no. 2, 1999.
- [10] L. Zhang and C. Meng, "Modeling of radiated noise passing characteristic for ship in different marine environments," *Proceedings of the International Conference on Materials Science and Applied Mechanics (MSAM)*, 2018.

Date of Received:
September 17, 2025

Date of Accepted:
September 25, 2025

Date of Published:
September 30, 2025
DOI: doi.org/10.30649/ijmea.v2i2.394

MATERIAL DURABILITY ANALYSIS ON FIBERGLASS SHIP CONSTRUCTION

Fariz Maulana Noor^{1*}

¹Hydrodynamics Technology Research Centre, National Research and Innovation Agency, Indonesia

*Corresponding Author: farizmaulana@gmail.com

ABSTRACT

Industrial needs for materials that have the same properties as metals and are resistant to corrosion require the development of various types of materials, one of which is fiberglass composite. The use of fiberglass material has been widely used in the automotive, shipping, and other industries. This research aims to analyze the strength of materials on fiber ships to identify the characteristics of FRP composite materials used on fiber ships. The method used in this research is to conduct material strength testing on FRP composite samples using tensile testing techniques to predict material strength on fiber ships. The results of the study are the highest tensile strength value, namely the volume fraction of 40%, namely 198.99 Mpa and the smallest tensile strength value at a volume fraction of 20% and the effect of tensile volume on tensile strength, where the greater the percentage of the volume fraction value, the greater the tensile strength value of the composite range from 20% to 40%. The conclusion in this study is that there is an effect of tensile volume on tensile strength, where the higher the percentage of volume fraction value, the higher the tensile strength value of the composite and in the test specimen almost debonding or fiber pull out, which occurs due to the selection of the manufacturing method, namely hand lay-up which is likely to occur voids in composite specimens.

Keywords: Endurance, fiberglass, materials, tensile test

Introduction

A fiber ship is one type of ship made of a fiber-reinforced plastic (FRP) composite material, which offers high strength and durability. Because fiber ships are made of composite materials, material strength analysis is critical to ensure the safety and reliability of the ship when operating at sea.

The use of composite materials, especially fiberglass, is already familiar in the shipping industry in Indonesia [1]. Fiberglass material is still the main choice for fishing boats, because regulations in Indonesia do not allow the use of wood raw materials as the basic material for shipbuilding, so fiberglass material is the main choice besides aluminum and steel [2].

The implementation of laminated fiberglass ship construction until now is still a special focus of both

practitioners and academics, where the thickness of the laminated layer does not guarantee that a fiberglass ship construction will be strong. Therefore, vulnerability in the hull construction section is a technological problem that must be solved [3].

Making fiberglass is not too difficult. The main material consists of three parts, namely fiber, resin, and catalyst [4]. This research intends to determine the strength, toughness, and hardness of fiberglass material based on fiber pattern variations by maintaining the composition of resin and catalyst.

This research aims to conduct a material strength analysis on fiber ships to identify the characteristics of FRP composite materials used in fiber ships, and evaluate the performance of fiber ships in terms of strength and resistance to external

loads such as water pressure and ocean waves. The method used in this research is to conduct material strength testing on FRP composite samples using tensile testing techniques to predict material strength on fiber ships.

The BKI Rules (1996 and 2009) do already include technical rules in ship building, but they still adopt the rules in foreign classification rules, where the basic water conditions used are different from the water conditions in Indonesia, which are relatively calm. Thus, rules on fiberglass ships still need to be refined and adapted to the conditions of Indonesian waters. Material usage standards are based on specimen test results (tensile strength, bending strength, and fiber content) according to the BKI 2006 rules. There are many types of -nonmarine grade|| fiberglass materials on the market at low prices, which are basically for use in making chairs, water tanks, children's toys, and others. Limited understanding and knowledge of the shipyard can result in the use of materials that are wrong and unqualified for use in shipbuilding. Some types of glass fiber and resin are on the market. Types of glass fibers in the local market include WR (Woven Roving), CSM (Chopped Strand Mat), and multiaxial of various sizes [4].

The results of this study are expected to provide a clear picture of the characteristics of FRP composite materials on fiber ships and also provide important information about the performance of fiber ships in terms of strength and resistance to external loads. This information can be a reference for ship companies to improve the quality and performance of their fiber ships, as well as maintain the safety of the ship and the crew working on it.

Thus, this material strength analysis research on fiber ships is expected to contribute to the development of ship technology and improve safety in the operation of fiber ships at sea.

However, there are still not many case studies to analyze material durability in fiberglass ship construction. So as to know the strength, toughness, and hardness. Therefore, in this case study, the analysis of material resistance in fiberglass ship construction. In this study, the authors developed a variety of fiber patterns by maintaining the composition of resin and catalyst.

Methodology

The method used in this research is to conduct material strength testing on FRP composite samples using tensile testing techniques to predict

material strength on fiber ships. For data collection by means of field observations and literature studies. For model design as follows:

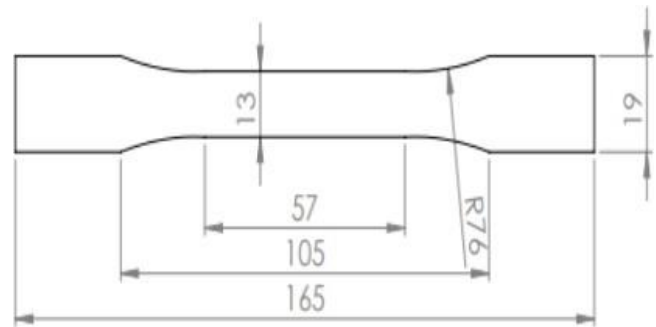


Figure 1. Model design

a. Model Sample

The sample making process uses the hand lay-up technique, where the sample is made with fiberglass fiber chopped standard mat and woven roving with fiber variations of 20%, 25%, 30%, 35%, 40%, 50%, 60%. The hand lay-up technique is one of the composite manufacturing. The process involves the manual placement of glass fiber (fiberglass) layers and impregnation with resin. First step: Place the first layer of glass fiber on a mold that has been coated with a separating agent. Then, apply resin using a brush or roller until the entire surface of the glass fiber is impregnated with resin.



Figure 2. Specimen: (a) CMS, (b) WR

Repeat this process for subsequent layers until the desired thickness is reached (Figure 1). Ensure that each layer of glass fiber (Figure 2) is well impregnated with resin and that no air bubbles are trapped. The advantages of this technique do not require sophisticated equipment and can be done at a relatively low cost; it can be used for a variety of

mold shapes and sizes, and the operator has full control over the amount of resin and fiber placement, allowing customization according to specific needs. However, product quality is highly dependent on the skill and experience of the operator; it is difficult to achieve consistent resin thickness and distribution, and the process can take longer than other, more automated techniques.



(a)



(b)

Figure 3. Tools and materials: (a) universal testing machine, (b) digital scales

b. Tools and Materials

In this study, several tools and materials are needed for testing purposes. Tools and materials used, such as a universal testing machine (UTM), a universal testing machine is mechanical devices used to perform a wide variety of tests on materials, including tensile tests, compression tests, bending tests, and more. Specimen molds are an important tool in the fiberglass composite manufacturing process, as they determine the shape, size, and final quality of the composite product. In the hand lay-up technique, molds are used to hold the glass fibers and resin during the forming and hardening

process. Digital scales are an essential tool in the process of making fiberglass composites using the hand lay-up technique. The main function of digital scales is to measure the weight of resin and other chemicals with high accuracy, ensuring the right ratio between components, which is crucial for the quality and consistency of the resulting composite tools and materials, as shown in Figure 3.

Collection techniques and data processing, and analysis. The research data is obtained from the results of tensile testing, and an analysis of the test results is carried out.

c. Tensile Test

Tensile testing is done to find stress and strain (stress-strain test). From this test, we can know some of the mechanical properties of materials that are needed in engineering design. The result of this test is a graph of load versus elongation. Load and elongation can be formulated (Eq.1 and Eq.2):

$$\sigma = \frac{F}{A_0} \quad (1)$$

where:

F = Load applied in the direction perpendicular to the cross section of the specimen (N)

A_0 = Initial cross-sectional area of the specimen before loading (m^2)

Σ = Engineering Stress (MPa)

$$\varepsilon = \frac{l_1 - l_0}{l_0} = \frac{\Delta L}{l_0} \quad (2)$$

ε = Engineering strain

l_0 = Initial length of specimen before loading (m)

ΔL = Length gain (m)

Tests are carried out by tensile testing of the matrix (plastic resin type) and the composite, using the JIS K 7113 (1981) testing standard (Annual Book of JIS Standards, K 7113, 396-407). Prepare a fiber with a minimum length of 10 cm according to the test standard. After that, make the paper shape, but in the middle, it is not broken. The tensile test specimen is placed between the paper then the end of the fiber is glued to the paper with adhesive glue. The purpose of sticking the fiber in the paper is so that the tensile load is only held by the fiber, so that the fiber retaining sheet only functions to hold the fiber, so that it does not slip with the clamp. After the paper sheet is clamped in the fiber tensile testing machine chuck, the fiber retaining sheet is

cut, so that the tensile load is only held by the fiber. Once ready, the test was carried out. The specimen is pulled until it breaks, and the load is recorded so that the tensile strength can be calculated and the maximum value.

d. Pull-Out Fiber Test

The tools and materials used for the pull-out fiber test include a single fiber with a predetermined length of at least 20 cm, a small pipe with a diameter of $\frac{1}{2}$ inch with a length of 3 cm, epoxy resin mixed with catalyst in a ratio of 100: 1 flat plate as a foundation, support pole so that the fiber can stand upright, fiber testing machine. universal with a maximum load of 10 kg, and adhesive glue.

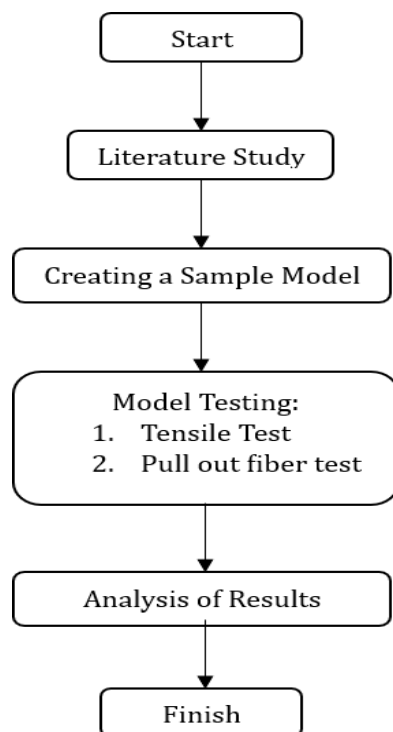


Figure 4. Flow chart

The initial step for working on the pull-out fiber test is to prepare a fiber with a minimum length of 20 mm that has been determined. Then, a small pipe that has been cut in a mold is placed on a flat plate with adhesive glue at the bottom of the pipe so that the epoxy resin does not leak. Tie the fiber to the support pole. Mix the matrix according to the dosage. Insert the fiber into the hole that has been made in the pipe with a fiber depth of 5 mm, 7 mm, respectively. After that, pour the matrix mixture into the prepared pipe mold where the fiber has been inserted first. Try to keep the mold surface

parallel to the poured resin. Place the specimen with the print on a flat surface, so that the position of the fiber can be perpendicular so that there is no tilt with the plate.

Wait for this condition for 8-12 hours or until the resin has completely dried. After all is done, pull-out fiber tests are carried out with a universal fiber testing machine with a maximum load of 10 kg.

After pull-out fiber tests are carried out, the critical length results will be obtained, and the fiber can be pulled out at a predetermined depth. This critical length is used as data for making composite fillers. The conceptual framework is shown in Figure 4.

Result and Discussion

Tensile testing results of fiberglass fiber composite material with polyester matrix, Yukalac series 157 BQTN-EX, with the influence of volume fraction.

Table 1 shows the results of the tensile and pull-out tests of glass fiber with variations in the ratio of fiber volume fraction and resin. The parameters measured are tensile strength (MPa), strain, and elastic modulus (GPa). Each variation of fiber and resin volume fraction is represented by five specimens (I- V).

Table 1. Tensile test results

Volume Fraction		Speciment	Stress (Mpa)	Strain	Elastic Modulus (Gpa)
Fiber (%)	Resin (%)				
40	60	I	207.82	30	2.99
		II	190.49	30	2.62
		III	156.18	19	2.9
		IV	195.67	23	2.9
		V	244.83	39	3.2
Average			198.99	28.2	2.93
35	65	I	162.68	47	2.7
		II	170.25	43	2.5
		III	172.04	37	2.4
		IV	151.90	27	2.6
		V	174.46	19	2.67
Average			166.26	34.6	2.59
30	70	I	152.49	19	2.57
		II	168.02	45	2.52
		III	133.73	21	2.49
		IV	150.73	30	2.40
		V	140.70	28	2.37
Average			149.13	28.6	2.47

25	75	I	143.39	33	2.25
		II	133.40	40	2.35
		III	120.29	68	2.04
		IV	111.33	41	1.93
		V	118.85	21	2.01
Average			142.28	40.6	2.12
20	80	I	102.95	32	2.12
		II	105.13	28	2.22
		III	111.75	24	2.24
		IV	119.43	25	2.16
		V	122.6	23	2.18
Average			112.37	26.4	2.18

Using a volume fraction of 40% fiber and 60% resin showed tensile strength results with an average of 198.99 MPa, with the highest value of 244.83 MPa (specimen V) and the lowest 156.18 MPa (specimen III). The strain value averaged 28.2%, with the highest strain of 39% (specimen V) and the lowest of 19% (specimen III). Meanwhile, the elastic modulus averaged 2.93 GPa, with the highest value of 3.2 GPa (specimen V) and the lowest 2.62 GPa (specimen II).

Using a volume fraction of 35% fiber and 65% resin showed tensile strength results with an average of 166.26 MPa, with the highest value of 174.46 MPa (specimen V) and the lowest 151.90 MPa (specimen IV). Strain values averaged 34.6%, with the highest strain of 43% (specimen II) and the lowest of 27% (specimen IV). Then, the elastic modulus has an average of 2.59 GPa, with the highest value of 2.77 GPa (specimen I) and the lowest of 2.5 GPa (specimen II). Using a volume fraction of 30% fiber and 70% resin showed tensile strength results with an average of 149.13 MPa, with the highest value of 168.02 MPa (specimen II) and the lowest of 133.73 MPa (specimen III). The strain has an average of 28.6%, with the highest strain of 45% (specimen II) and the lowest of 21% (specimen III). Meanwhile, the elastic modulus averaged 2.49 GPa, with the highest value of 2.57 GPa (specimen I) and the lowest 2.37 GPa (specimen V).

In testing using a volume fraction of 25% fiber and 75% resin, the tensile strength value has an average of 142.28 MPa, with the highest value of 143.39 MPa (specimen I) and the lowest of 111.33 MPa (specimen IV). The strain values showed an average of 40.6%, with the highest strain of 41% (specimen IV) and the lowest of 23% (specimen III). Then, the elastic modulus has an average of 2.12 GPa, with the highest value of 2.25 GPa (specimen I) and the lowest of 2.01 GPa (specimen V). Using a

volume fraction of 20% fiber and 80% resin, the tensile strength had an average of 112.37 MPa, with the highest value of 119.43 MPa (specimen IV) and the lowest of 102.95 MPa (specimen I). Meanwhile, the strain value has an average of 26.4%, with the highest strain of 32% (specimen V) and the lowest of 23% (specimen I). It has an elastic modulus value with an average of 2.18 GPa, with the highest value of 2.24 GPa (specimen II) and the lowest 2.16 GPa (specimen IV).

The highest tensile strength was found at 40% fiber volume fraction and 60% resin, while the lowest tensile strength was found at 20% fiber volume fraction and 80% resin. The highest strain is found in the volume fraction of 25% fiber and 75% resin, while the lowest strain is found in the volume fraction of 20% fiber and 80% resin. The highest elastic modulus was found at 40% fiber volume fraction and 60% resin, while the lowest elastic modulus was found at 25% fiber volume fraction and 75% resin. In general, increasing the fiber volume fraction tends to increase tensile strength and elastic modulus, but has a mixed effect on strain.

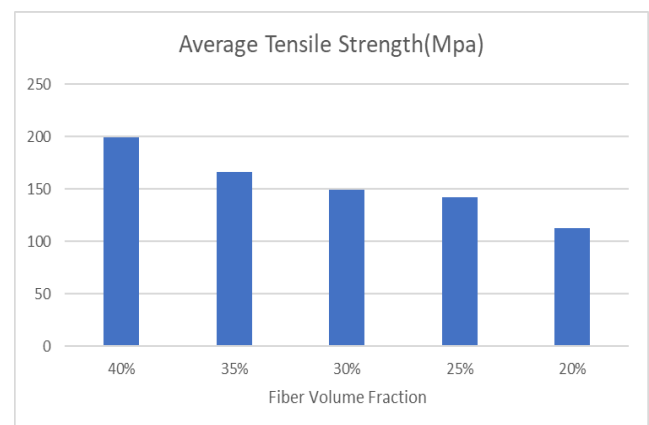


Figure 5. Comparison of the tensile strength of fiberglass composites against volume fraction

The variation of volume fraction based on the figure above has an influence on the tensile strength. The 40% fraction got a tensile strength of 198.99 MPa, the 35% fraction got a tensile strength of 166.266 MPa, the 30% fraction got a tensile strength of 149.134 MPa, the 25% fraction got a tensile strength of 142.282 MPa, and the 20% fraction got a tensile strength of 110.918 MPa. From the test results, it is known that the highest tensile value is at 40% fraction and the lowest is at 20% fraction, meaning that there is an effect of volume fraction on the composition of composite materials, where the strength increases as the volume of fiber

increases. This tensile strength is influenced by alkali treatment, which can remove natural matrices such as hemicellulose, lignin, wax, and oil, which affect the fiber surface.

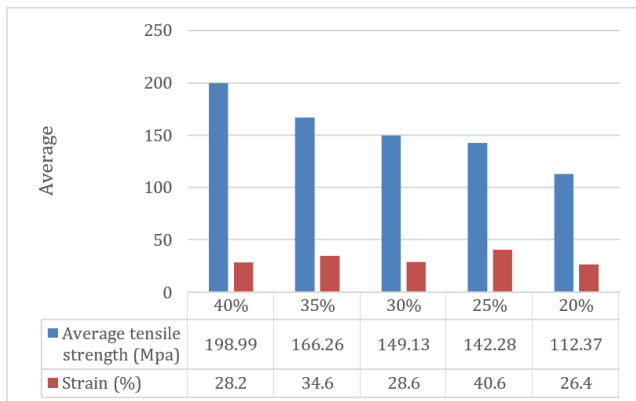


Figure 6. Stress and strain graph of fiberglass fiber composite

Figure 6, the stress and strain of fiberglass fiber composite material with polyester matrix, Yukalac series 157 BQTN-EX, with the influence of volume fraction, can be seen in Figure 5. The fractions used are 40% volume fraction, 35% volume fraction, 30% volume fraction, 25% volume fraction, and 20% volume fraction. Fiber composites with a volume fraction of 40% have a tensile strength of 198.99 MPa as the maximum stress with a maximum strain of 28.2% so that an elastic modulus of 2.9314 GPa is obtained. The fiber composite with a volume fraction of 35% has a tensile strength of 166.266 MPa as the maximum stress with a maximum strain of 34.6% so that an elastic modulus of 2.5916 GPa is obtained. The fiber composite with 30% volume fraction has a tensile strength of 149.134 MPa as the maximum stress with a maximum strain of 28.6% so that an elastic modulus of 2.4754 GPa is obtained. The fiber composite with a volume fraction of 25% has a tensile strength of 142.282 MPa as the maximum stress with a maximum strain of 40.6% so that an elastic modulus of 2.1228 GPa is obtained. The fiber composite with 20% volume fraction has a tensile strength of 110.918 MPa as the maximum stress with a maximum strain of 29.2% so that an elastic modulus of 2.22175 GPa is obtained. Then, the tensile tests for volume fractions of 40%, 50%, and 60% are shown in Figure 7 below.

Figure 7 above shows that the increase in tensile load occurs in composites with fiber volume fractions of 40%, 50% and 60%. The composites with 50% and 60% fiber volume fraction have a

tensile load of 5749.3 N, which is greater than the tensile load of the composite with 40% fiber volume fraction, which is 4512.6 N.

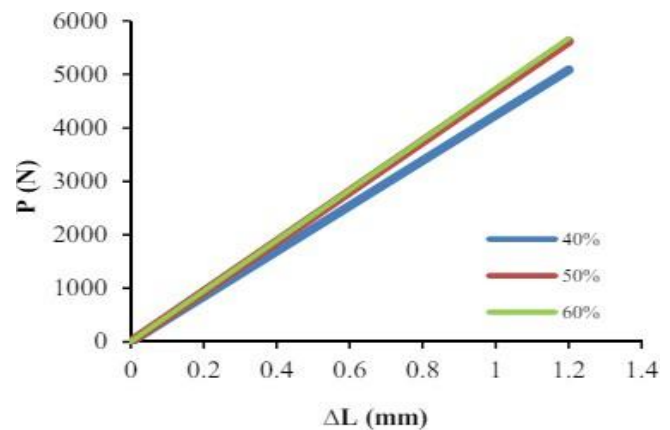


Figure 7. Relationship graph between load P (N) and length increase ΔL (mm) of 40%, 50%, and 60% volume fraction

The tensile load of the composite with 40% fiber volume fraction has the lowest value, with a length increase of 1.2 mm. The relationship between stress and strain due to tensile loading can be seen in the graph in Figure 8 below.

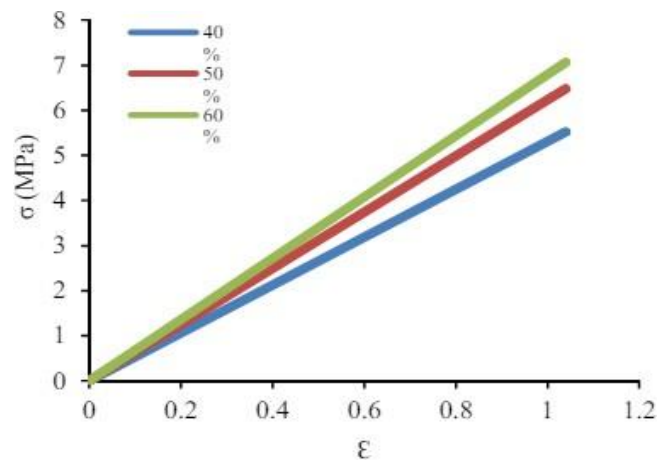


Figure 8. Relationship between stress (σ) and strain (ϵ)

From Figure 8 above, it can be seen that variations in fiber volume fractions of 40%, 50% and 60% influence the resulting tensile stress. The increase in tensile stress occurs from 40% fiber volume fraction to 50% fiber volume fraction and 60% fiber volume fraction, so that the 60% fiber volume fraction has the highest tensile stress of 7.2 MPa. This shows that increasing the fiber volume fraction can increase the amount of load transferred by the fiber as reinforcement. This is also because the mat works well in binding an increasing number of fibers, accepting the load and passing it on to the fibers as

reinforcement. The graph of the relationship between elastic modulus and volume fraction variation of the nylon-polyester composite material is shown in Figure 9.

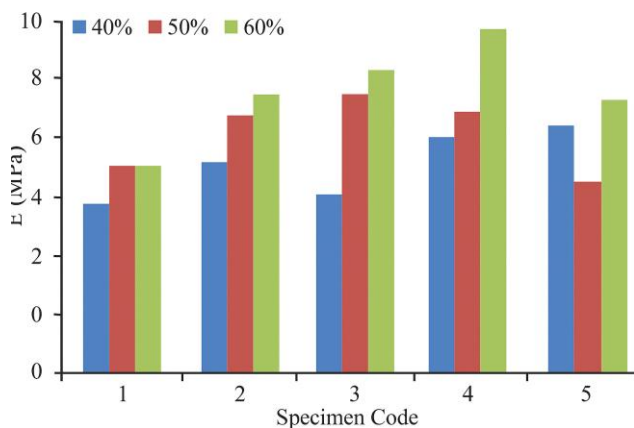


Figure 9. Relationship between modulus of elasticity and fiber volume fraction 40%, 50%, 60%

From Figure 9, it is found that increasing the volume fraction can also increase the stiffness of the material as indicated by its elastic modulus value. This is because the elastic modulus value is directly proportional to the stress value, so that with increasing stress, the elastic modulus also increases. The increase in stress value with increasing fiber volume fraction also increases the stiffness of the matrix because it is reinforced by many fibers. This is also shown by the damage mechanism that occurs, caused by the fiber pull-out mechanism. Fiber pull-out damage indicates that the matrix is strong enough to withstand the initial load so that matrix crack damage does not occur. As the testing load increases, greater load transfer occurs to the fiber as reinforcement. When the load reaches a certain point, the fibers bonded by the matrix break away from their interfacial bonds, so the visible composite damage is fiber pullout.

Conclusion

Based on the results of research and data analysis that has been carried out by varying the value of the volume fraction in the composite, it can be concluded that in the variation of the volume fraction (40%, 35%, 30%, 25%, and 20%) the results obtained are the highest tensile strength value of the 40% volume fraction, namely 198.99 Mpa and the smallest tensile strength value is at a volume fraction of 20%. Based on the test results, it is found that the effect of volume fraction on tensile strength, where the higher the percentage of

volume fraction value, the higher the tensile strength value of the composite in the range of 20% to 40%. In each test specimen, debonding or fiber pull-out almost occurs, which occurs due to the selection of the manufacturing method, namely hand lay-up, which is likely to cause voids in the composite specimen.

The strain and modulus of elasticity also vary with the fiber volume fraction. Higher fiber content generally leads to a higher modulus of elasticity but has a mixed effect on strain. The highest strain was observed at a 25% fiber volume fraction, indicating that this composition allows for more elongation before breaking. The highest modulus of elasticity was noted at the 40% fiber volume fraction, suggesting a stiffer material compared to other compositions.

Meanwhile, the fracture patterns of tensile testing composites at 40%, 50% and 60% fiber volume fractions show brittle properties and mechanisms (fiber pull out). The pull-out fiber test revealed that debonding or fiber pull-out is a potential issue, particularly influenced by the manufacturing technique. Proper control during the hand lay-up process is crucial to minimize these defects.

References

- [1] S. A. Carli, Widyanto, and H. Ismoyo, "Analysis of tensile and bending strength of woven-type glass fiber composite with epoxy and polyester matrix in symmetrical layers using hand lay-up manufacturing method," *Universitas Diponegoro*, Semarang, 2012.
- [2] R. N. Ichsan and I. M. Arif, "Effect of composite laminate arrangement reinforced by E-glass and carbon fiber on tensile strength with polyester matrix," *JTM*, vol. 3, no. 3, 2015.
- [3] B. Ma'ruf and Farief, "Technology of fiberglass ship construction," *SBU Marine, PT Biro Klasifikasi Indonesia*, Jakarta, 2016.
- [4] B. Ma'ruf, "Analysis of hull laminate strength of fiberglass ships using multiaxial material," *Jurnal Standardisasi BSN*, vol. 16, no. 1, pp. 77–84, 2014.
- [5] B. Ma'ruf, "Study on the standardization of fiberglass ship hull laminate construction," *Jurnal Standardisasi BSN*, vol. 13, no. 1, pp. 16–25, 2011.
- [6] F. Rusmiyatno, "Effect of fiber volume fraction on tensile and bending strength of nylon/epoxy resin random short-fiber composites," *Universitas Negeri Semarang*, 2007.
- [7] I. Marzuki, A. Zubaydi, and B. Ma'ruf, "Study on the application of classification rules in fiberglass fishing vessel hull structure laminates (3 GT)," *Wave: Jurnal Ilmiah Teknologi Maritim*, vol. 11, no. 1, pp. 15–22, 2017.

- [8] W. T. Nugroho, "Effect of fiber model on the strength, toughness, and hardness of fiberglass material," *Jurnal Ilmiah Inovasi*, vol. 15, no. 1, 2015.
- [9] A. Alam, R. J. Ikhwan, and T. Hidayat, "Strength of fiberglass reinforced plastic (FRP) as a frame material for wooden ships," *Wave: Jurnal Ilmiah Teknologi Maritim*, vol. 15, no. 1, pp. 1–10, 2021.
- [10] Tim Fakultas Teknik Universitas Negeri Yogyakarta, *OPKR-60-029A Module: Fabrication of fiberglass/composite components*, 2004.
- [11] R. G. Fardhana and E. Sugianto, "Strength analysis of sandwich material made of plastic bottles and sengan wood powder for waste collection vessel hull," *Universitas Hang Tuah*, Surabaya, 2023.
- [12] R. Fadilah and G. Widyaputra, "Analysis of tensile strength and microstructure of composite material on PROSOE KMHE 2019 electric car body," *Jurnal Teknik Mesin*, vol. 9, no. 2, 2020.
- [13] E. D. Sulistyowati, "Effect of fiber length and volume fraction on impact and bending strength of polyester-fiber glass and polyester-pandan wangi composites," *Jurnal Keilmuan dan Terapan Teknik Mesin*, vol. 2, no. 1, 2012.
- [14] A. Alam, R. J. Ikhwan, and T. Hidayat, "Comparison effect of resin and catalyst on tensile strength of polyester fiberglass composite for shipbuilding materials," *Jurnal Inovasi Sains dan Teknologi Kelautan*, vol. 1, no. 2, 2020.
- [15] A. H. Siregar, B. A. Setyawan, and A. Marasabessy, "Fire-resistant fiberglass-based FRP composite as ship body material," *Jurnal Ilmiah Fakultas Teknik UPN "Veteran" Jakarta*, vol. 12, no. 2, 2016.
- [16] A. Nurudin, "Potential development of continuous laminated hibiscus tiliaceus fiber-reinforced composites as a fiberglass substitute for ship hull fabrication," *Jurnal Keilmuan dan Aplikasi Teknik*, vol. 12, no. 2, 2011.
- [17] P. P. Tambunan, H. Yudo, and P. Manik, "Technical analysis of laminated board of petung bamboo fiber and fiberglass woven roving for ship hull skin material," *Jurnal Teknik Perkapalan UNDIP*, vol. 10, no. 2, 2022.
- [18] H. Yudo and S. Jatmiko, "Technical analysis of mechanical strength of bagasse fiber-reinforced composite material in terms of tensile and impact strength," *Jurnal Ilmu Pengetahuan dan Teknologi Kelautan*, vol. 5, no. 2, 2008.

Date of Received:
September 17, 2025

Date of Accepted:
September 28, 2025

Date of Published:
September 30, 2025
DOI: doi.org/10.30649/ijmea

DESIGN OF THE MAIN ENGINE FOUNDATION OF SHIP X TO SUPPORT MAIN ENGINE REPOWERING

Agil Thoriq Ramadhani^{1*}, Sutrisno¹

¹ Department of Marine Engineering, University of Hang Tuah, 60111, Indonesia

*Corresponding Author: agilthoriqram@gmail.com

ABSTRACT

Ship "X" is one of the motor ships built in 1974 and is of the passenger type. Repowering is planned because the current speed is deemed insufficient to meet the expected operational targets. The ship uses the previous main engine with a capacity of 4 x 1340 HP to 2 x 2600 HP. An important part of the main engine is the foundation located at the bottom, because the foundation is attached to the main engine with a large power, the foundation must effectively ensure the safety of the hull structure to withstand a wide variety of forces that can be provided by loads on the foundation. The engine foundation must be able to withstand the load on it without causing shear stress, as if the engine has become an integral part of the ship itself. Given that this will be done, a new main engine foundation design process will be made. There are two types of materials simulated, namely bki grade A and B standard steel, with two loads during operation, namely a fixed load of 29,577.15 N and a total load of 165,128.41 N. In carrying out the research, modeling and simulation were carried out with Autodesk Inventor software. So, this research produces the most efficient material, namely bki grade A steel, because it has a greater yield strength and tensile strength. The material has simulation results with minimal and maximum difference values in %, Stress XY 0.56%, Stress Z 0, 11%, Stress YY 0.11%, Stress stress and strain of Von Mises Stress 0.05%, 1st Principal Stress 0.18%, 3rd Principal Stress 0.18%, Stress XX 0.03YZ 0.02%, Stress ZZ 0.07, Equivalent Strain 0.44%, 1st Principal Strain 0.46%, 3rd Principal Strain 12.25%, Strain XX 0.02%, Strain XY 0.18%, Strain XZ 0.09, Strain YY 0.22%, Strain YZ 0.36%, Strain ZZ 0.09%.

Keywords: Design, foundation, main engine, load, repowering, strain, strength, stress

Introduction

Ships are used as a means of sea transportation for goods, people, and services delivered by ship [1]. Ship X is a motor ship built in 1974 and sails under the Indonesian flag. The ship is a Roll-on/Roll-off (Passenger Ro-Ro) type, functioning as a passenger ship with destinations from Garongkong Port, Barru, South Sulawesi, to Paciran Port, Lamongan.

East Java. The ship renovation plan includes changing the main engine (repowering) from the original main engine with a capacity of 4 x 1340 HP to a main engine of 2 x 2600 HP. Renovations are also being carried out on the ship's accommodation

section located above the vehicle deck, including the addition of capsule rooms for passengers, the addition of passenger service areas such as a gym, karaoke, barbershop, cafeteria, massage room, and open area [2]. Therefore, the main use of Ro-Ro ships is as a means of transportation, including off-road vehicles such as cars and trucks, as well as land transportation [3].

Repowering is still frequently carried out, although it is not the primary engineering choice. The main reason for this is the demand for stable ship performance, which includes meeting service speeds, economical ship operations, and uninterrupted performance. This occurs while ship

owners do not have sufficient funds to build new ships [4]. Engines with high power require double base construction and a strong engine foundation so that the forces generated by the engine during operation can be absorbed. The engine foundation must be able to withstand the superimposed loads without causing shear or crushing failure. The shear stress that occurs on perpendicular planes must have zero components [5]. In ship construction, the engine foundation is very important because it bears the load from the main engine, the force from the propeller, and the vibration from the main engine [6].

To ensure the safety of the ship's hull structure, the main engine foundation must be able to withstand various variations in force that can place loads on the foundation. The engine foundation helps keep the engine upright in its position as if it were part of the ship. The foundation must be able to withstand deformation due to loads within the permissible limits if the drive motor foundation and the surrounding base structure have sufficient rigidity [7]. The engine foundation must be installed with special care so that the engine shaft axis and the propeller shaft axis are always straight [8].

Based on the above description, there is a need for research on the design of the main engine foundation on ship X to support this repowering. As there is no such research yet, the author proposes the title "Design of the Main Engine Foundation of Ship X to Support Main Engine Repowering". This research uses simulation with Autodesk Inventor Professional 2021 software to analyze the strength of the main engine foundation with different material specifications. This research aims to determine the load received by the new main engine foundation for the repowering plan on passenger ships, calculate the strength of the foundation with several material specifications, and the stress caused by the main engine.

Methodology

The methodology used in this research is a design method using AutoCAD software to create the construction form of the main engine foundation of ship X to support the repowering of the main engine. The model will then be tested for strength using simulations with Autodesk Inventor Professional 2021 software with material variations to determine which material is suitable. After that, it will be validated using manual

calculations in accordance with applicable guidelines and standards.

The simulation results with static analysis were produced by Autodesk Inventor. Static analysis uses the finite element method and aims to determine whether the frame design and materials used are safe. This determines the stress on materials and structures that experience static or dynamic loads or forces. This condition is achieved if the stress that occurs does not exceed the yield strength. If the stress exceeds the yield strength, it will not return to its original shape when subjected to static loads. The Von Mises criterion determines whether a combination of stresses will cause failure. Von Mises stress is also known as equivalent stress. Principal stress indicates the maximum and minimum normal stresses that occur in a material during complex loading conditions. Determining the principal stress can reveal the most severe stress concentration when the material is subjected to multi-directional stress, which is very important for preventing structural failure. A perpendicular plane has zero shear stress components on that plane.

Two types of principal stress will be discussed here: First Principal Stress and Third 3rdPrincipal Stress [5]. Meanwhile, strain is when an object changes in size due to a force or couple in equilibrium compared to its initial size. Strain, also known as the degree of deformation, is measured to determine the amount of deformation when mechanical stress occurs. This produces a measure of the force that occurs, such as load and stress. In addition, it is used to calculate the strength and safety value of a material or structural component that contains it, which affects the safety factor. The Safety Factor is used to assess the safety of a frame. The safety factor can be determined either at the most extreme elastic stress or at the yield stress of the material. The safety factor is used to evaluate a design with the least assessment. The material and frame design are considered safe if the minimum value produced by the material and frame is not more than one [5].

In conducting this research, data related to the issues discussed in this study are required. In collecting this data, the observation method was used, which is data collection carried out by directly observing an object using the five senses. The data obtained will be used as a reference in the process of working on this research. During the implementation of this research, data collection was carried out to complete this proposal, both

from the internet and from previous studies. The data collected for this proposal includes ship data such as overall length (LOA), ship height (H), ship width (B), ship draft (T) as shown in Table 1, engine room dimensions, new main engine specifications, new main engine dimensions, marine gear specifications, plate dimensions, plate specifications, and plate composition as shown. The ship used as the object of research in this study is a Ro-Ro passenger ship, as shown in Table 1.

Table 1. Main ship data

No	Parameter	Symbol	Value
1	Total Length (m)	LOA	88,91
2	Length Perpendicular (m)	LPP	84,00
3	Waterline Length (m)	LWL	3,7
4	Maximum Width (m)	B	15,80
5	Height (m)	H	5,54
6	Water Depth (m)	T	3,70
7	Service Speed (knot)	Vs	15.25

Table 1 shows the main data of the ship that will be used for this study, namely, a passenger ship. The main ship data includes Length Over All (LOA), Length between Perpendicular (LPP), Length Water Line (LWL), Breadth (B), Height (H), Draft (T), Service Speed (Vs) [2].

Table 2. Engine room dimensions

No	Parameter	Value (m)
1	Length	23.4
2	Width	11.4
3	Height	5.54
4	Length for main engine	7.4

Table 2 shows the dimensions of the engine room that will be used for this study. The dimensions of the engine room are a key parameter in the construction of the main engine foundation because the dimensions of the main engine to be used are different from those of the previous main engine.

Table 3. New main engine

No	Parameter	Value
1	Brand	Yanmar 6EY26W
2	Type	4-stroke, Diesel
3	Piston Stroke (mm)	385
4	Piston Speed (m/s)	9.63
5	Number of Cylinders	In-line 6

6	Cylinder Bore (mm)	260
7	MEP (MPa)	1.92–2.50
8	Rated Output (PS)	2610
9	Rated Engine Speed (rpm)	750
10	Dry Weight (kg)	18500

Table 3 shows the specifications of the new main engine [9], which will be used to determine the forces that will be generated in designing the main engine foundation of the ship. These main gine specifications are used to calculate the forces that will be exerted and input into the software setup that will determine the engine undation model.

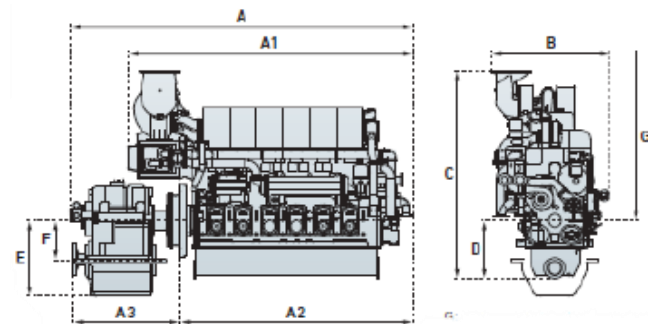


Figure 1. Main engine dimensions

Table 4. Main engine dimensions value

No	Parameter	Value (mm)
1	A	5601
2	A1	4271
3	A2	3563
4	A3	2070
5	B	1804
6	C	3112
7	D	842
8	E	555
9	F	—
10	G	1900

Figure 1 and Table 4 show the dimensions of the new main engine [9] that will be used for this study. The dimensions of this new main engine are the main parameters for designing the engine foundation, starting from a two-dimensional design and developing it into a three-dimensional one.

Table 5. Marine gear specifications

No	Parameter	Value
1	Marine Gear Model	Yanmar YXH 2500C
2	Propeller Type	F.P.P.

3	Reduction Gear Ratio (Forward)	2.23, 2.58, 2.79, 3.03
4	Marine Gear Dry Weight (kg)	4800
5	Total Dry Weight with Marine Gear (kg)	23840

Table 5 shows the specifications of the marine gear [9] that will be used to complete this study. These marine gear specifications serve as supplementary data in this study.

Table 6 shows the dimensions of the plate that will be used for this study. These plate dimensions are used in the plate size for designing the machine foundation model. The specification is shown in Table 7. Table 8 shows the composition of the plate that will be used to complete this study. The composition of the plate affects the specifications of the plate that will be used.

Table 6. Plate dimensions

No	Parameter	Value
1	Thickness (mm)	4 – 25
2	Width (mm)	300 – 2000
3	Length (mm)	1250 – 12500
4	Weight (kg)	875 – 2625
5	Pallet Weight (Metric Ton)	6

Table 7. Plate specifications

No	Specification	Value
1	Grade	A
2	Yield Strength (MPa)	292 min.
3	Tensile Strength (MPa)	430
4	Elongation (%)	28 min.
5	Impact Energy (Joule)	Not specified

Table 8. Composition of plate content

No	Element / Content	Value (%)
1	Carbon (C)	0.1721
2	Silicon (Si)	0.195
3	Manganese (Mn)	0.520
4	Phosphorus (P)	0.108
5	Sulfur (S)	0.0087
6	Chromium (Cr)	0.014
7	Nickel (Ni)	0.007
8	Copper (Cu)	0.015
9	Molybdenum (Mo)	0.001
10	Vanadium (V)	-

a. Calculation of Load Received by the Foundation

The stage of calculating the load that will be received by the ship's main engine foundation using

formulas and provisions by the Indonesian Classification Bureau (BKI). The calculation of the main engine foundation load is based on the weight of the main engine and the forces that will be generated when the engine is operating.

b. Main Engine Load

The main engine load is generated from the weight of the main engine, which is distributed evenly on the foundation and is also influenced by the torque/rotation of the engine with a vertical load reaction. This vertical load increases the engine load on one side and reduces the main engine load by the same value on the other side.

$$\begin{aligned}
 W_{\text{mainengine}} &= \text{Weight} \times \text{Gravity} \\
 &= 3015 \text{ kg} \times 9.81 \text{ m/s}^2 \\
 &= 29577.15 \text{ N/m}
 \end{aligned}$$

c. Torsional Load on the Shaft

The shaft functions as a power transmitter from the engine to the propulsor. The power transmitted by the shaft is in the form of torsional moment. Several calculations must be performed to determine the torsional load on the shaft.

d. Main Engine Foundation Construction Calculations

The thickness of the construction is calculated in accordance with the Indonesian Classification Bureau, as in Table 8, Rules for Hull Volume II Edition 2009, Section 6. The depth of plate floors, the web thickness is not to be less than:

$$T = h100 + 4,0 \text{ s (mm)}$$

Where:

h = floor plate depth according to section A.1.2.1.

Table 9. Engine bed thickness

No	Plate	Dimensions (thickness × width × length)
1	Krakatau Steel	35 × 325 × 4550

Plate floors shall be installed on each frame. The longitudinal girders of the engine seating are to be supported transversely by means of web frames or wing bulkheads. The scantlings of web frames are to be determined according to Section 9, A.6. Floor thickness according to B.6.2. The thickness of the longitudinal beams above the inner base in Table 9

from the assembly results using Autodesk Inventor Professional.

Figure 7 shows the meshing stage with a face size of 0.1 mm, which produced 568,881 elements and 304,159 nodes from the results of converting the mesh view using Autodesk Inventor Professional.

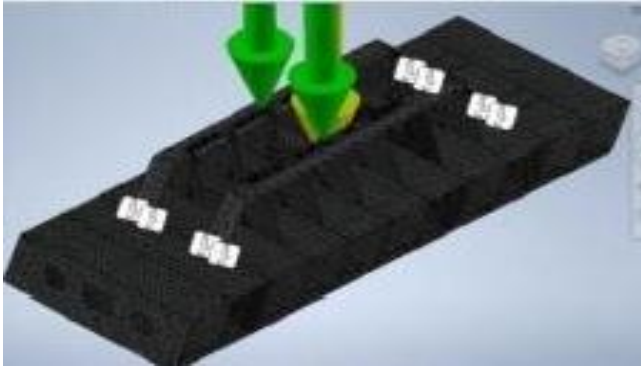


Figure 7. Mesh view display of the engine foundation

The setup process is the most important process because all parameters for the simulation are processed at this stage. There are many things that must be done to determine the boundary conditions in relation to a simulation. Here are some things that need to be set in the setup process, as shown in Table 10.

The following is the physical material setup in the main engine foundation model with varying material specifications. Figure 8 shows the physical material model with grade A steel with a yield strength of 282 MPa and a tensile strength of 441 MPa, and Figure 9 shows grade B with a yield strength of 235 MPa and a tensile strength of 400 MPa.

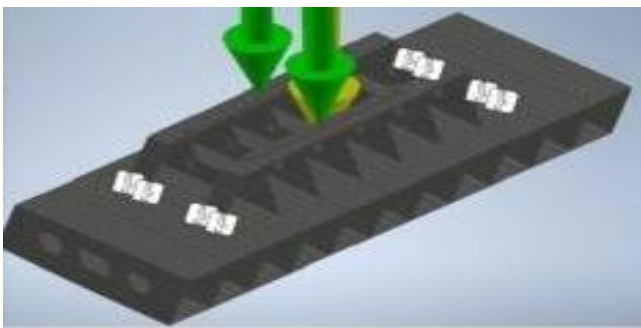


Figure 8. Physical material model of steel grade A

Table 10. Engine setup

No	Force / Stress	Value
1	Gravity	9.81 m/s ²

2	Force	29,577.15 N
3	Torsional Shaft Force	13,555,126.097 N

Result and Discussion

The simulation results from Autodesk Inventor Professional software on the steel grade A and B foundation models were used to determine the strength of the foundation (load, stress received by the foundation, and safety factor).

a. The Effect of Constant Loading on Stress and Strain

Analysis results of stress and strain on the main engine foundation material with variations in BKI steel grades A and B under a load of 29,577.15 N. To facilitate the analysis process, probe coordinates were assigned in the form of letters A, B, C, and D to determine the amount of stress at each point.

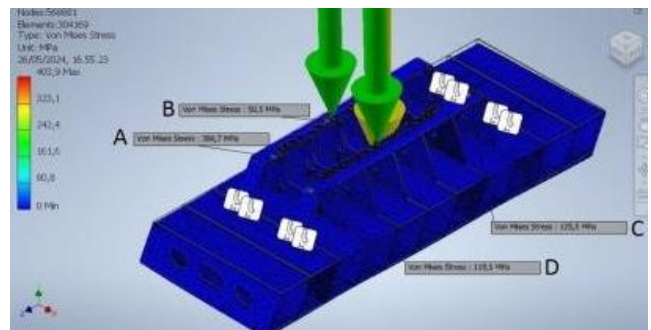


Figure 9. Von mises stress model A for constant loading

Table 11. Probe points for stress values in models A and B

Stress Type	A (MPa)	B (MPa)	C (MPa)	D (MPa)
Von Mises Stress	352.9	53.7	128.6	120
1st Principal Stress	406.6	-1.2	65.3	125.1
3rd Principal Stress	28.1	-57.8	-82.7	-6
Stress XX	115.9	-2.5	24.1	22.8
Stress XY	-88.4	-2.3	6.9	-7.1
Stress XZ	26.73	-2.4	-49.37	13.6
Stress YY	345.2	-7.2	-1.8	24.6
Stress YZ	-100.9	6.3	-45.4	-54.8
Stress ZZ	60.3	-57	-37.7	92.2

Table 11 shows the probe points (A, B, C, and D) of the four probes, indicating the main locations

where stress occurs. The stress values are at the lower frame, the center of the engine bed, and the engine bed bend reinforcement of model A under constant loading.

Table 12 shows the probe points (A, B, C, and D) of the four probes, indicating the main locations of strain occurrence. The strain values are at the lower frame, the middle of the engine bed, and the engine bed bend reinforcement of model A under constant loading.

b. The Effect of Total Loading on Stress and Strain

The results of the stress and strain analysis on the main engine foundation material with variations in BKI grade A and B steel material under a load of 165,128.41 N. To simplify the analysis process, only the total load was compared because the results showed significant differences. Probe coordinates were labeled A, B, C, and D to determine the amount of stress at each point.

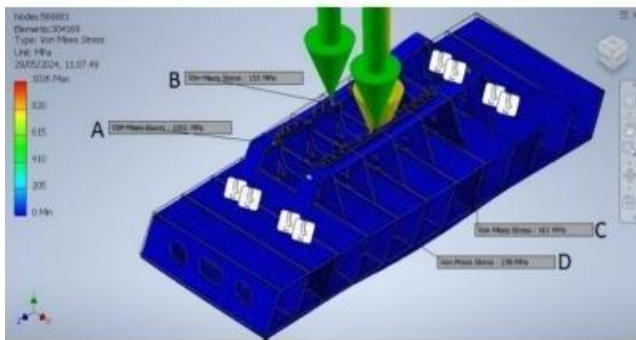


Figure 10. Von misses stress model A for total loading

Figure 10 shows an example of the Von Mises stress results on BKI grade A steel material with a load of 165,128.41 N. The green arrow indicates the direction of the load acting directly above the engine bed, and the yellow arrow indicates the assumed direction of gravity. The minimum von Mises stress is 0 MPa, and the maximum is 1026 MPa. The von Misses stress color indicator ranges from blue to red; the closer the color is to red, the higher the von Misses stress value. For the results of 1st Principal Stress, 3rd Principal Stress, Stress XX, Stress XY, Stress XZ, Stress YY, Stress YX, Stress ZZ, and equivalent strain values, 1st Principal Strain, 3rd Principal Strain, Strain XX, Strain XY, Strain XZ, Strain YY, Strain YZ, and Strain ZZ, with the difference will be presented in Table 11.

Table 13. Comparison of model A results for total loading

Results	Model A (Maximum)
Von Mises Stress	1026 MPa
1st Principal Stress	1109 MPa
3rd Principal Stress	195.1 MPa
Stress XX	343.5 MPa
Stress XY	232.7 MPa
Stress XZ	188.3 MPa
Stress YY	943.7 MPa
Stress YZ	432.6 MPa
Stress ZZ	427.7 MPa
Equivalent Strain	0.00450601 μl
1st Principal Strain	0.00506355 μl
3rd Principal Strain	0.0000426485 μl
Strain XX	0.00132967 μl
Strain XY	0.00149032 μl
Strain XZ	0.0019083 μl
Strain YY	0.00459041 μl
Strain YZ	0.00250916 μl
Strain ZZ	0.00150500 μl

The comparison data for model A in Table 13 shows that the simulation results for grade A bki plate material are in good agreement with the simulation results, showing significant results.

Table 14. Comparison of probe point A under constant loading

Results	Model A (Point A)
Von Mises Stress	962 MPa
1st Principal Stress	989 MPa
3rd Principal Stress	-77.6 MPa
Stress XX	198.8 MPa
Stress XY	-91.7 MPa
Stress XZ	44.2 MPa
Stress YY	904 MPa
Stress YZ	-265.9 MPa
Stress ZZ	-4.2 MPa
Equivalent Strain	0.004259 μl
1st Principal Strain	0.004910 μl
3rd Principal Strain	-0.001784 μl
Strain XX	-0.000266 μl
Strain XY	-0.000587 μl
Strain XZ	0.000283 μl
Strain YY	0.004248 μl
Strain YZ	-0.001427 μl
Strain ZZ	-0.001565 μl

The comparison data for probe point A in Table 14 shows that the simulation results in Autodesk Inventor Professional software are significant.

Table 15. Comparison of probe point B total load

Results	Model A (Point B)
Von Mises Stress	167 MPa

1st Principal Stress	0 MPa
3rd Principal Stress	-168.4 MPa
Stress XX	-3.9 MPa
Stress XY	-0.1 MPa
Stress XZ	1 MPa
Stress YY	-0.1 MPa
Stress YZ	5 MPa
Stress ZZ	-168.2 MPa
Equivalent Strain	0.000733 μl
1st Principal Strain	0.000345 μl
3rd Principal Strain	-0.000782 μl
Strain XX	0.000216 μl
Strain XY	-0.000001 μl
Strain XZ	0.000006 μl
Strain YY	0.000241 μl
Strain YZ	-0.000001 μl
Strain ZZ	-0.000836 μl

Table 16. Comparison of probe point C total load

Results	Model A (Point C)
Von Mises Stress	156 MPa
1st Principal Stress	167 MPa
3rd Principal Stress	2.7 MPa
Stress XX	47.4 MPa
Stress XY	-7.4 MPa
Stress XZ	-56.7 MPa
Stress YY	4.2 MPa
Stress YZ	5.4 MPa
Stress ZZ	139.9 MPa
Equivalent Strain	0.00064 μl
1st Principal Strain	0.000805 μl
3rd Principal Strain	-0.00026 μl
Strain XX	0.000035 μl
Strain XY	-0.000047 μl
Strain XZ	-0.000363 μl
Strain YY	-0.000241 μl
Strain YZ	-0.000030 μl
Strain ZZ	0.000628 μl

The comparison data for probe point B in Table 15 shows that the simulation results in Autodesk Inventor Professional software are significant. Moreover, the comparison data for probe point C in Table 16 shows that the simulation results in Autodesk Inventor Professional software are significant. Furthermore, the comparison data for probe point D in Table 17 shows that the simulation results in Autodesk Inventor Professional software are significant.

Table 17. Comparison of probe point D total load

Results	Model A (Point D)
Von Mises Stress	267 MPa
1st Principal Stress	277 MPa
3rd Principal Stress	-13.6 MPa
Stress XX	48.1 MPa

Stress XY	-13 MPa
Stress XZ	25.7 MPa
Stress YY	53.9 MPa
Stress YZ	-121.8 MPa
Stress ZZ	206.2 MPa
Equivalent Strain	0.001182 μl
1st Principal Strain	0.001375 μl
3rd Principal Strain	-0.000535 μl
Strain XX	-0.000124 μl
Strain XY	-0.000083 μl
Strain XZ	0.000165 μl
Strain YY	-0.000086 μl
Strain YZ	-0.000560 μl
Strain ZZ	0.000888 μl

c. Safety Factor Analysis

Safety factor analysis results for the main engine foundation material with variations in BKL grade A and B steel materials against the load received. To simplify the process, probe coordinates are given in the form of letters A, B, C, and D to determine the amount of stress at that point.

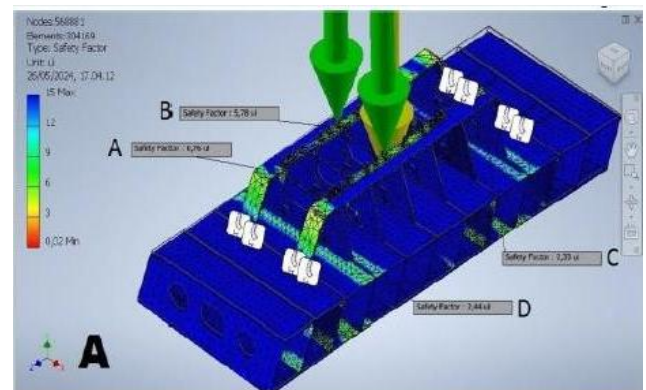


Figure 11. Safety factor A with constant loading

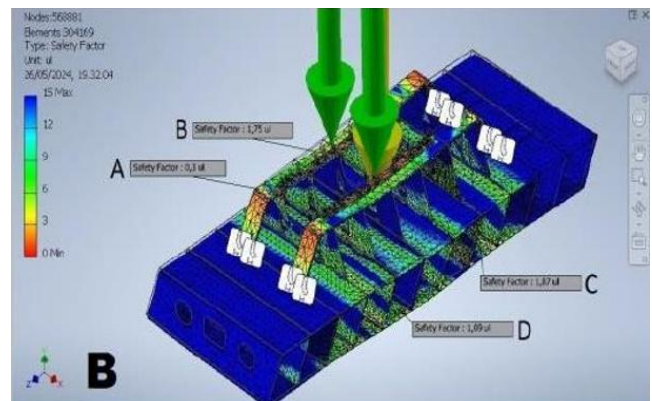


Figure 12. Safety factor A with total loading

Figures 11 and 12 show the safety factor around the main engine foundation with two variations of material model A, with fixed and total loading. The

color representation starts from the bottom color, which is red, and the top color, which is blue. The higher the color, the greater the safety factor. Therefore, the bluer the color, the safer it is, and the redder the color, the more dangerous the safety factor of the material is.

The data on the safety factor of material model A in Table 18 shows that the simulation results in Autodesk Inventor Professional software have significant differences in each probe in the safety factor of the two models, namely, probe point A 30.43%, probe point B 15.89%, probe point C 30.43%, and probe point D 25.29%.

Table 18. Safety factor comparison

Results	Model A
Probe Point A (μl)	0.30
Probe Point B (μl)	1.75
Probe Point C (μl)	1.87
Probe Point D (μl)	1.09

Conclusion

For the construction of the main engine foundation for repowering planning by comparing one BKI-standard plate material to determine stress and strain, it can be concluded that:

- The calculated static load is 29,577.15 N. The calculated total load is 165,128.41 N.
- The specifications of the material used for the main engine foundation model comparison are very influential due to the differences in the chemical composition mixture used in forming the steel plate, and the yield strength and tensile strength figures are very influential.
- The yield strength and tensile strength values in model A are 292 MPa and 430 MPa.
- The percentage comparison values of stress and strain show a significant difference, with a maximum simulation result difference and at 4 probe points, with a maximum stress result of 0.87% and strain of 0.44%. Then, at probe point A, the stress of the two models was 51.93%, with a difference in strain between the two models of 30.45%. At probe point B, the stress of the two models was >100%, with a difference in strain between the two models of >100%.
- At probe point C, the stress of both models was 48.15%, with a strain difference between the two models of 87.97%. At probe point D, the stress of both models was 5.82%. The

strain difference between the two models was 44.11%.

- The minimum safety factor value is 0 μl and the maximum is 15 μl. Both models have 4 probe points for comparison of results: probe point A 30.43%, probe point B 15.89%, probe point C 30.43%, probe point D 25.29% with the highest safety level in model A at point A 0.3 μl, point B 1.75 μl, point C 1.87 μl, point D 1.09 μl.

Acknowledgments

On this occasion, the author would like to express his deepest gratitude and appreciation to Allah SWT for His guidance and blessings, to all the lecturers of the marine engineering department at Hang Tuah University who have imparted their knowledge during the course of study, and to PT. Adiluhung Sarana Segara Indonesia for assisting in this research. Therefore, suggestions and input are needed to improve and advance this work.

References

- [1] S. A. Fitri, "Optimization of Propeller Selection Due to Engine Replacement for the Charma Rucitra 3 Ship," *ITS Repository*, 2023. [Online]. Available: <http://repository.its.ac.id/id/eprint/97017>
- [2] L. Pekerjaan, "Technical Specifications," pp. 1–10, 2014.
- [3] M. A. Asis, "Faculty of Engineering, Hasanuddin University Gowa 2020," 2020. [Online]. Available: <http://repository.unhas.ac.id/id/eprint/1828/>
- [4] S. Federico and H. N. Wibowo, "Performance Study of Fast Boat Engines After Re-Powering," *ResearchGate*, vol. 02, no. 05, p. 2017, 2012.
- [5] F. S. Perdana, A. Akbar, and H. Mahmudi, "Analysis of Material Strength and Frame of a 1.2-Ton Cattle Rolling Device Using Autodesk Inventor Software," *J. Semin. Nas. Inov. Teknol.*, pp. 1–7, 2022.
- [6] K. M. Y. Emily, N. A. Nugroho, and P. Herijono, "Info Articles Abstract," vol. 2, no. 1, pp. 2021–2022, 2021. [Online]. Available: <http://e-journal.ivet.ac.id/index.php/maristec>
- [7] S. Jokosisworo and E. Widiyanto, "Analysis of Machine Foundation Strength on Mt. Nsl-Iv Due to Changes in Main Engine Capacity at Pt. Jasa Marina Indah Using the Finite Element Method," *Kapal*, vol. 8, no. 2, pp. 79–81, 2012.
- [8] Biro Klasifikasi Indonesia, "Section 20 Fatigue Strength," *Rules Hull 2019 Edition*, vol. II, pp. 20–7, 2019.
- [9] Yanmar, "Marine Diesel Engine Products Guide: Limitless Blue Skies and Oceans."

Date of Received:
September 23, 2025

Date of Accepted:
September 29, 2025

Date of Published:
September 30, 2025
DOI: doi.org/10.30649/ijmea.v2i2.393

SUSTAINABLE MARITIME HUMAN RESOURCE DEVELOPMENT STRATEGY IN SUPPORTING THE BLUE ECONOMY IN INDONESIA

Dedi Kristiawan¹, Sugeng Marsudi^{2*}

¹ Ship Operation Technology Study Program, Hang Tuah University, 60111, Indonesia

² Marine Machinery Engineering Technology Study Programs, Hang Tuah University, 60111, Indonesia

*Corresponding Author: sugeng.marsudi@hangtuah.ac.id

ABSTRACT

The development of maritime human resources (HR) is a key factor in realizing a sustainable blue economy in Indonesia. However, there are fundamental gaps in the form of an educational curriculum that is not fully relevant to industry needs, limited access to ongoing training, and low ownership of international certifications among the maritime workforce. This study aims to analyze the actual conditions, main obstacles, and strategies for strengthening maritime HR competencies to increase national and global competitiveness. The research method used a quantitative descriptive survey of 128 respondents, consisting of sailors, cadets, maritime vocational education lecturers, industry practitioners, and regulators in Surabaya, Makassar, and Bitung, supplemented by in-depth interviews. The results showed that 72% of respondents considered the curriculum not yet in line with the demands of the blue economy, 64% stated that ongoing technical training was still limited, and only 38% had international certification. A SWOT analysis identified priority strategies, namely strengthening the blue competency-based curriculum, on-demand training according to industry needs, vocational-industry partnerships, and digitalization of the training and certification system. In conclusion, maritime human resource development requires an integrated approach between the government, educational institutions, and industry to create an adaptive, competent, and sustainable workforce, in line with Indonesia's vision as the world's maritime axis.

Keywords: Blue economy, competence, maritime education, strategy, human resources

Introduction

The Blue Economy concept has emerged as a transformative development paradigm emphasizing the balance between economic growth, environmental preservation, and social welfare. As the world's largest archipelagic nation, Indonesia possesses immense maritime potential spanning fisheries, shipping, marine tourism, and ocean-based energy. Nevertheless, this potential remains underutilized due to limited qualified human resources (HR), weak institutional coordination, and insufficient innovation [1][4][9].

GINANJAR and ADRIYADI [1] emphasized that human resource optimization is vital to support the Blue Economy in Riau Islands Province,

highlighting the need for capacity enhancement in maritime sectors. PURBA [3] further asserted that sustainable maritime industry growth depends on continuous human capital development that aligns with sustainability and digital transformation principles. Meanwhile, HADININGRAT et al. [7] noted that modernizing sea transport and logistics is fundamental for realizing the "Golden Indonesia 2045" vision based on maritime resilience and innovation. Hence, the sustainable development of maritime HR is central to Indonesia's economic transformation. Strengthening technical competence, environmental literacy, and managerial capacity, supported by sustainable

policy integration, is crucial for the successful implementation of the Blue Economy [6][16].

The urgency of this study arises from Indonesia's need to build an adaptive and future-ready maritime workforce in the face of global economic and technological shifts. Although the government has introduced the Blue Economy Roadmap, its implementation remains hindered by fragmented coordination and a lack of professional expertise in marine sustainability [12][14]. Maqfirah and Laba [6] highlighted that the journey toward "Golden Indonesia 2045" requires synergy between innovation, vocational education, and policy coherence. Thus, developing a comprehensive maritime HR strategy is essential to ensure human resource quality that meets industrial demand while preserving marine ecosystems as a sustainable economic foundation.

Recent literature indicates a paradigm shift in Indonesia's Blue Economy, from resource exploitation to sustainable, innovation-driven management. Hendarman et al. [2] presented a systematic review outlining the necessity of integrating technology, policy, and HR development to achieve sustainability. Marwa et al. [4] identified education quality, regulatory efficiency, and technological advancement as key determinants of Blue Economy growth. Trenggono et al. [16] expanded this view by highlighting the role of innovation ecosystems and research-based collaboration between universities and maritime industries to produce environmentally conscious professionals. Globally, Anikwe et al. [10] discussed similar HR challenges in Nigeria's Blue Economy, reinforcing that sustainable human capacity development is a global priority for achieving marine-based economic resilience.

The novelty of this study lies in formulating an integrated sustainable maritime HR development strategy through three main dimensions: green-technology-oriented technical competencies. Sustainability-based maritime vocational education and cross-sectoral policy collaboration between academia, industry, and government. Unlike prior studies that primarily focused on macroeconomic or environmental aspects of the Blue Economy, this research develops a strategic human resource framework tailored to Indonesia's maritime context [5][7][13]. The study contributes a new conceptual model for capacity development that aligns national maritime competitiveness with sustainability objectives.

A number of previous studies have examined the intersection of the Blue Economy and human resource development in Indonesia and beyond. Sari and Muslimah [11] underscored the need for blue economy policies to promote sustainable fisheries management. Muliando et al. [12] discussed strategies for fulfilling the need for fisheries supervisors, emphasizing HR's critical role in effective policy implementation. Sabrina and Putra [8] analyzed Indonesia's regional initiatives in ASEAN, emphasizing cross-border cooperation to promote sustainable fisheries practices.

Wuwung et al. [9] evaluated Indonesia's sustainable ocean development policies, positioning them as pathways to achieving a maritime-oriented economy. Silalahi et al. [5] explored the transformation of the Blue Economy in strengthening the defense economy, linking maritime sustainability to national security. Furthermore, Ginanjar and Adriyadi [1] focused on HR optimization in the Riau Islands, while Andana and Saputra [13] proposed regional policy diversification to maximize maritime potential through Indonesia-China cooperation. Yusuf et al. [14] conducted a sustainability analysis of fisheries and marine resources, stressing the integration of social and ecological dimensions in Blue Economy frameworks. At the international level, Purba [3] and Anikwe et al. [10] highlighted that sustainable human capital remains the core driver for Blue Economy advancement in developing countries. Their findings confirm that investment in education, digital literacy, and sustainability-oriented training programs determines the success of maritime sectors globally. These studies collectively suggest that while Indonesia has initiated various Blue Economy policies, a comprehensive HR development model integrating technical, environmental, and institutional dimensions remains underdeveloped — a gap that this research seeks to address.

The research objectives are to analyze the current condition and challenges of maritime HR development in Indonesia's Blue Economy framework. Moreover, to formulate a Sustainable Maritime Human Resource Development Strategy that supports Indonesia's national maritime vision and the Golden Indonesia 2045 agenda.

Methodology

a. Research Design

This research adopts a mixed-methods design, combining qualitative and quantitative approaches

to obtain a comprehensive understanding of the implementation and optimization of the Blue Economy in Indonesia. The qualitative aspect focuses on exploring policies, institutional coordination, and stakeholder perceptions, while the quantitative component analyzes economic, environmental, and social indicators relevant to maritime sectors.

The study aims to answer three main questions:

- How ready are Indonesia's maritime regions in implementing Blue Economy principles?
- What are the main challenges in integrating human resources, digitalization, and policy frameworks?
- What strategies can strengthen the sustainability and competitiveness of Indonesia's maritime economy?

A descriptive-explanatory approach was selected to explain the causal relationships between human resource capacity, institutional readiness, and sustainable maritime development outcomes.

b. Research Location and Object

The research was conducted across three representative maritime regions:

- Riau Islands Province — representing western Indonesia's maritime trade and fisheries sector.
- East Java Province — representing central maritime logistics and port operations, including Tanjung Perak Port.
- North Sulawesi Province — representing eastern Indonesia's marine tourism and aquaculture industries. These regions were chosen because they reflect the diversity of Indonesia's maritime potential and provide insight into various Blue Economy dimensions such as fisheries, shipping logistics, shipyard operations, and marine tourism.
- Population and Sample - The population includes all stakeholders involved in Blue Economy implementation in Indonesia. A purposive sampling technique was used to select respondents who possess relevant expertise and authority. Government officials from the Ministry of Marine Affairs and Fisheries and the Ministry of Transportation. Port authorities and shipping company representatives are involved in maritime logistics. Local

community leaders and coastal entrepreneurs engaged in fisheries and eco-tourism. Academics and maritime policy experts provide analytical perspectives. In total, 30 key informants were interviewed to represent multi-sectoral viewpoints.

c. Data Collection Techniques

– Primary Data

Primary data were collected using semi-structured interviews and field observations. Interviews were guided by a list of open-ended questions exploring perceptions about Blue Economy implementation, human resource challenges, digital readiness, and environmental management practices. Field observations were conducted in selected ports, fishing communities, and maritime training centers to assess on-site sustainability initiatives.

– Secondary Data

Secondary data were obtained from official government documents (e.g., Indonesia's Blue Economy Roadmap, National Marine Policy Reports). Academic journals and proceedings, including works by Ginanjar & Adriyadi [1], Hendri & Wibowo [2], and Sukmana et al. [3]. Statistical databases, such as the Central Bureau of Statistics (BPS), the Ministry of Marine Affairs and Fisheries, and UNDP's Blue Economy Index dataset.

d. Research Instruments

To ensure validity and reliability, the study utilized:

- Interview guidelines validated by maritime policy experts.
- Observation checklists focusing on sustainability indicators (energy efficiency, waste management, and digital port systems).
- Questionnaire instruments with Likert-scale items to measure perceptions of readiness and sustainability.
- Pilot testing was conducted to refine the instruments and minimize interpretation bias.

e. Data Analysis Techniques Qualitative Analysis

Qualitative data were analyzed using thematic analysis with the following steps:

- Data reduction — categorizing information based on recurring themes (policy

integration, human resource capacity, technology adoption).

- Coding and interpretation — identifying relationships between institutional readiness and Blue Economy success.
- Triangulation — comparing interview data with secondary documents to ensure consistency and credibility

f. Quantitative Analysis

Quantitative data were processed using descriptive and inferential statistics.

- Descriptive statistics were applied to evaluate the performance of key indicators (e.g., GDP contribution from maritime sectors, number of trained maritime workers, and environmental quality index).
- Inferential tests (e.g., correlation analysis) were used to identify relationships between human capital, policy integration, and sustainability outcomes.

All quantitative analyses were conducted using Microsoft Excel and SPSS to ensure accuracy and transparency.

g. Research Framework

The conceptual framework integrates three interrelated dimensions supporting Blue Economy development:

- Human Capital Dimension — focuses on maritime education, competency certification, and workforce adaptation to sustainable practices.
- Policy and Institutional Dimension — examines the alignment and coordination between central and regional maritime policies.
- Digital and Environmental Innovation Dimension — evaluates the adoption of green technologies and digital transformation within ports, fisheries, and logistics.

The interaction among these dimensions forms the analytical basis for identifying strategic recommendations toward an integrated and sustainable Blue Economy ecosystem in Indonesia.

Result and Discussion

The majority of respondents (68.75%) assessed the competency of Indonesia's maritime human resources at an intermediate level. Only 18.75% considered their competency to be high, while 12.5% stated it was still low. This data indicates

that despite progress, the majority of the maritime workforce is not yet fully prepared to meet the demands of the blue economy, which emphasizes efficiency, sustainability, and digitalization. In other words, there remains a significant gap between actual competency and global standards.

Table 1. Competency level of maritime human resources in Indonesia

Competency Categories	Number of Respondents	Percentage (%)
Tall	24	18.75
Intermediate	88	68.75
Low	16	12.50
Total	128	100

Table 2. Access to ongoing training

Access Category	Number of Respondents	Percentage (%)
Regularly attend training	35	27.34
Limited access to training	75	58.59
Never attended training	18	14.06
Total	128	100

A total of 58.59% of respondents stated that their access to training remains limited. This is especially true for active seafarers outside Java, who are constrained by distance, cost, and program availability. Only 27.34% regularly attend training annually, while 14.06% have not attended any training in the past five years. This data demonstrates the urgent need to expand access to digital technology-based training, such as e-learning or blended training, to achieve equitable competency.

Table 3. HR development strategies are considered the most effective

Human Resource Development Strategy	Number of Respondents	Percentage (%)
Industry-based training	51	39.84
Vocational partnerships-maritime industry	42	32.81

Digitalization of training & certification	22	17.19
National maritime human resources roadmap	13	10.16
Total	128	100

The most frequently chosen strategy by respondents was industry-needs-based training (39.84%), followed by vocational-industry partnerships (32.81%). This confirms that direct collaboration between maritime education and the workplace is considered key to improving competency. Meanwhile, digitalization of training (17.19%) and the development of a national roadmap (10.16%), although lower, remain important as long-term supporting strategies. These results demonstrate that a human resource development approach cannot be partial but requires a combination of strategies that integrate education, industry, and government.

The findings of this study highlight that Indonesia's transition toward a Blue Economy depends critically on the integration of human resource development, institutional governance, and digital-environmental innovation. These three dimensions form a mutually reinforcing system that determines the country's ability to balance economic growth with marine ecosystem sustainability.

a. Integration with SWOT Analysis

Based on the results of surveys, interviews, and documentation, the most effective maritime human resource development strategies can be summarized in four main recommendations:

- Enhancement of the blue competency-based curriculum to align with STCW standards and global industry needs.
- Strengthening partnerships between vocational education and the maritime industry through link and match programs.
- Development of digital technology-based training to expand access and overcome geographical barriers.
- Preparation of a national maritime human resource development roadmap as a long-term guideline.

b. Human Resource Competence as the Foundation of the Blue Economy

The empirical data show that the lack of trained and certified maritime workers poses a major barrier to sustainable maritime operations. Only 46% of Indonesia's maritime workforce has obtained competency certification or sustainability-oriented training. This aligns with Ginanjar & Adriyadi [1], who emphasize that human resource optimization is a strategic driver of regional Blue Economy success in the Riau Islands.

Purba [3] also argued that human capital development—through education, technical training, and long-term investment in skills—is vital for marine industry competitiveness. Similarly, Anikwe et al. [10] observed that workforce training and re-skilling programs are directly correlated with economic resilience in maritime economies.

This study extends these findings by showing that, beyond technical training, digital literacy and environmental awareness are equally essential competencies for maritime workers. For example, in East Java, digital monitoring of port emissions and waste management practices was significantly more effective when personnel had prior environmental training. Hence, developing sustainable maritime HR must go beyond conventional seafaring skills to include knowledge of energy efficiency, data management, and ecosystem protection.

c. Policy Integration and Institutional Coordination

Policy analysis revealed fragmented implementation across government levels. Despite the establishment of Indonesia's Blue Economy Roadmap (2023–2045), inconsistencies between national and regional regulations persist. These findings support Hendarman et al. [2] and Marwa et al. [4], who identified overlapping mandates among ministries as a major obstacle to achieving integrated maritime governance.

However, the present study finds that policy coherence can be improved through the Triple Helix model, involving collaboration among government, academia, and industry. For instance, the partnership between Universitas Hang Tuah, local fisheries agencies, and private port operators in East Java has resulted in measurable improvements in port energy efficiency and fishery certification compliance.

Andana & Saputra [13] further noted that regional diversification policies under bilateral cooperation with China have enhanced the

competitiveness of the Riau Islands. This reinforces that institutional synergy—supported by shared data platforms, joint training initiatives, and standardized evaluation systems—is crucial for effective Blue Economy governance.

d. Innovation, Digitalization, and Environmental Transformation

Technological innovation emerged as the most dynamic aspect of Indonesia's Blue Economy development. Evidence from field observations shows the successful implementation of smart port technologies at Tanjung Perak and eco-fisheries systems in North Sulawesi. These innovations reduced logistics time by 25% and decreased plastic waste by 15%, respectively.

Trenggono et al. [16] highlighted that technological adaptation and innovation are necessary to strengthen environmental sustainability in the marine and fisheries sectors. Similarly, Wuwung et al. [9] argued that digital transformation—when integrated with environmental policies—can catalyze achieving Indonesia's maritime vision.

The study contributes to this discourse by providing empirical evidence that digital innovation amplifies environmental outcomes only when accompanied by trained personnel and institutional coordination. For example, the application of automated waste monitoring at ports proved ineffective in areas lacking trained environmental officers, illustrating that technology alone cannot substitute human and institutional capacity.

e. Toward a Sustainable Maritime Human Resource Strategy

Synthesizing these findings, the research proposes a Sustainable Maritime Human Resource Development Framework, consisting of three strategic pillars:

- Competency and Certification Alignment – Updating maritime education curricula to align with IMO standards and sustainability competencies.
- Integrated Institutional Governance – Establishing a national Maritime Human Resource Council to coordinate HR policies across ministries.
- Digital-Ecological Integration – Embedding environmental sustainability and digital readiness in maritime workforce training programs.



Figure 1. Maritime human resources development strategy

Conclusion

This framework for achieving Golden Indonesia 2045 requires inclusive human and institutional transformation. Moreover, it also emphasized that Blue Economy transformation is not only economic, but also strategic for national defense and sovereignty. Further study is required to emphasize the findings.

Acknowledgments

This section is optional. List the names of institutions or individuals who provided assistance during the research here, for example, those who provided capital, those who helped with language preparation, provided assistance as proof of reading articles, etc.

References

- [1] A. Ginanjar and A. Adriyadi, "Optimization of Human Resources (HR) to Support Blue Economy in Riau Island Province," *Journal of Maritime Policy Science*, vol. 1, no. 3, pp. 110–118, 2024.
- [2] A. F. Hendarman et al., "Current research and future perspectives: A literature review on the blue economy of Indonesia," in *BIO Web of Conferences*, vol. 92, p. 01030, EDP Sciences, 2024.
- [3] J. T. Purba, "Strategy optimizing marine industry through sustainable human capital development: Indonesia perspectives," *Mediterranean Journal of Social Sciences*, vol. 6, no. 5, pp. 129–135, 2015.
- [4] T. Marwa, Muizzuddin, A. Bashir, S. Andaiyani, and A. Cahyadi, "Determinants of the blue economy growth in the era of sustainability: A case study of Indonesia," *Economies*, vol. 12, no. 11, p. 299, 2024.
- [5] A. D. H. Silalahi, P. Suwarno, and D. Hermanto, "Blue Economy Transformation to Realize Defense Economy," *Asian Journal of Management, Entrepreneurship and Social Science*, vol. 5, no. 4, pp. 249–271, 2025.

- [6] M. Maqfirah and A. R. Laba, "The Role of Blue Economy Towards Golden Indonesia 2045," in *9th Int. Conf. on Accounting, Management, and Economics 2024 (ICAME 2024)*, pp. 2010–2018, Atlantis Press, July 2025.
- [7] K. S. S. Hadiningrat, B. Wiradanti, and Y. F. Umar, "Transformation of Indonesian Sea Transportation and Maritime Logistics to Realize The Vision of Golden Indonesia 2045," *Jipower: Journal of Intellectual Power*, vol. 1, no. 1, pp. 89–107, 2024.
- [8] O. Sabrina and R. A. Putra, "Navigating the Blue Economy: Indonesia's Regional Efforts in ASEAN to Support Sustainable Practices in Fisheries Sector," *Sustainability*, vol. 17, no. 15, p. 6906, 2025.
- [9] L. Wuwung, A. McIlgorm, and M. Voyer, "Sustainable ocean development policies in Indonesia: paving the pathways towards a maritime destiny," *Frontiers in Marine Science*, vol. 11, p. 1401332, 2024.
- [10] S. O. Anikwe, L. C. Unachukwu, and F. N. Onah, "Human capacity development and sustainable growth in the blue economy: Opportunities, challenges, and strategies for Nigeria," *African Banking and Finance Review Journal*, vol. 15, no. 15, 2024.
- [11] D. A. A. Sari and S. Muslimah, "Blue economy policy for sustainable fisheries in Indonesia," in *IOP Conf. Ser.: Earth and Environmental Science*, vol. 423, no. 1, p. 012051, IOP Publishing, 2020.
- [12] T. B. Mulianto, A. Asropi, and R. Rajab, "Strategy to Fulfill The Need For Fisheries Supervisors To Support The Ministry Of Marine Affairs And Fisheries' Blue Economy Policy," *Eduvest-Journal of Universal Studies*, vol. 4, no. 12, pp. 12199–12220, 2024.
- [13] F. Andana and C. F. W. B. Saputra, "Regional Policy Diversification to Maximize Blue Economy Potential in Kepulauan Riau Amid Indonesia-China Bilateral Cooperation," *Journal of Maritime Policy Science*, vol. 2, no. 1, pp. 13–25, 2025.
- [14] M. Yusuf, A. D. Riana, R. Rusneni, W. A. Salawali, and E. Eddiwam, "Sustainability analysis of fisheries and marine resource development in Indonesia's blue economy framework," *Biodiversitas Journal of Biological Diversity*, vol. 26, no. 7, 2025.
- [15] H. Prasutiyon and R. Tambun, "The Contribution of the Maritime Sector to Economic Development," 2025.